Anion Photoelectron Spectroscopy and High Level Calculations of the Halide–Methanol Clusters

Hannah Adam

Supervisor: Dr Duncan A. Wild

Honours Thesis submitted as part of the B.Sc. (Hons) degree

The School of Molecular Sciences

The University of Western Australia

Date of Submission: 03/11/17

Declaration

I certify that the material of this thesis has not been submitted for any other award or degree at any institution.

I certify that, to the best of my knowledge, any sources used in this thesis and any help received have been acknowledged within this thesis.

_____

Hannah Adam, November 2017

Acknowledgements

This research was undertaken with the assistance of computational resources from the Pople high-performance computing cluster of the Faculty of Science at the University of Western Australia.

This research project would not have come to completion without all the tremendous effort, help and numerous Dad jokes from my supervisor Duncan Wild. Thank you Duncan for the opportunity to be a part of the Wild group, for the chance to 'play with the machine' and for the many times you reminded me that yes, I can do this. It has been a fun and educational year, one that I will never forget. Thanks also goes to Amir Karton, who stepped in and cleared up our misconceptions on complete basis set extrapolations. You saved us hours of debate and provided us with a solid understanding of the correct techniques to be used. Thank you to the workshop staff of the Bayliss Building, whose speedy skills made it possible to keep experiments running.

I would also like to thank Peter, Tim and Christian, for helping me adjust to the lab and for always being happy to explain a concept. I couldn't have gotten through the year without our 'Dominoes Tuesdays' and 'Dirty Burger Fridays' and the occasional good natured work place bullying.

Finally, to my family and friends, who didn't understand what I was doing but put up with my constant worrying none the less and provided endless amounts of moral support.

Abstract

Halide - methanol interactions were studied using coupled Time of Flight - Mass Spectrometry and Photoelectron Spectroscopy complemented with ab initio calculations within the context of atmospheric chemistry. Photoelectron spectra were produced for chloride - methanol, bromide - methanol and iodide - methanol complexes, with binding and stabilisation energies found. These energies confirmed that the halide - methanol complexes are more stable, meaning the electron is more tightly bound to the complexes than the bare halide. Computational data supported these findings, and geometries were also elucidated, finding one anion stationary point and two neutral stationary points.

Contents

List of Abbreviations

CBS . . . . . Complete Basis Set

CC . . . . . Coupled Cluster Theory

CCSD(T) . . . . . Coupled Cluster Theory with Single, Double and Perturbative Triple Excitations

CFCs . . . . . Chlorofluorocarbons

EA . . . . . Electron Affinity

HF . . . . . Hartree - Fock

HPMS . . . . . High Pressure Mass Spectrometry

MP2 . . . . . Second Order Mϕller - Plesset Perturbation Theory

PES . . . . . Photoelectron Spectroscopy

SEVI . . . . . Slow Electron Velocity-Map Imaging

SPE . . . . . Single Point Energy

TOF . . . . . Time of Flight

TOF-MS . . . . . Time of Flight - Mass Spectrometry

TOF-MS/PES . . . . . Time of Flight - Mass Spectrometry/Photoelectron Spectroscopy

TOF-PES . . . . . Time of Flight - Photoelectron Spectroscopy

VDE . . . . . Vertical Detachment Energy

Chapter 1

Introduction

Intermolecular interactions play an important role in chemistry. From simple dissociation to complex synthesis reactions, an understanding of the way species interact and react with one another is vital to almost all areas of chemical study. With this in mind, the primary objective of this project will be to study the intermolecular interactions between halogens and the simplest alcohol, methanol, keeping in mind their importance in atmospheric chemistry. The project will proceed through a synergy between experimental and computational methods. This chapter will set out the theory behind these techniques and give greater insight into the purpose behind this project. For the remainder of the thesis, halogen complexes refer to the neutral complexes while halide complexes refer to the anion complexes.

1.1 van der Waals Clusters

Van der Waals clusters occur when ions, atoms or molecules in the gas phase interact, thereby forming weak intermolecular bonding structural motifs.[1] These fragile clusters are useful for studying the pre-reaction adducts or transition state regions of reaction potential energy surfaces, as these stages in chemical reactions are unstable and difficult to pin-point experimentally.[1] This project will therefore concentrate on van der Waals clusters of methanol and the halogens chlorine, bromine and iodine, which will allow the properties of such clusters to be determined and aid in understanding the reaction dynamics of these systems. An example of the chloride - methanol cluster is given in Figure 1.1.

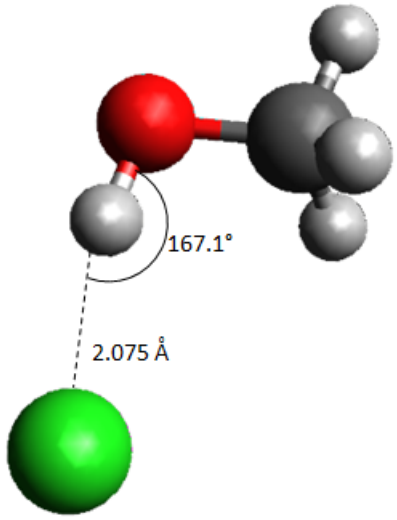

Figure 1.1: Chloride . . . methanol cluster optimised at the MP2/aug-cc-pV(Q+d)Z level of theory

1.2 Atmospheric Chemistry

The reasoning behind studying the intermolecular forces between methanol and halogens is due to their relevance in the field of atmospheric chemistry, an area of chemistry that affects human life. This direct impact creates the desire to better comprehend our atmosphere, the species within it and their interactions and reactions. This project aims to contribute towards this field of study.

1.2.1 Atmospheric Halogens

Halogens have a well-documented existence in the atmosphere and their known atmospheric sources include chlorofluorocarbons (CFCs)[2] and the marine boundary layer.[3] Additionally, their contribution to the destruction of the ozone layer has been well researched,[4] which is the primary reason for continuing the investigation of halogens in our atmosphere. When halogens react with certain species in the atmosphere, they can form undesirable reservoir species that when subjected to light will release a free halogen radical, which goes on to destroy the ozone. This reaction pathway is shown below.[4]

$$\cdot \mathrm{X} + \mathrm{O_3} \longrightarrow \cdot \mathrm{XO} + \mathrm{O_2} \tag{1.1}$$

·X in this case would be a halogen radical and ·XO, the reservoir species, would then continue on to take part in reactions such as

$$\cdot \mathrm{XO} + \cdot \mathrm{XO} \longrightarrow \cdot \mathrm{X} + \cdot \mathrm{X} + \mathrm{O_2} \tag{1.2}$$

$$\cdot \mathrm{XO} + \mathrm{H_2O} \longrightarrow \mathrm{XOH} + \cdot \mathrm{OH} \tag{1.3}$$

$$\mathrm{XOH} + \mathrm{h}\upsilon \longrightarrow \cdot \mathrm{X} + \cdot \mathrm{OH} \tag{1.4}$$

This known involvement in catalytic ozone destruction highlights the importance of halogen interactions with atmospheric species. In particular, the interactions of halogens with methanol, another known atmospheric species, will be the focus of this project.

1.2.2 Atmospheric Methanol

Methanol is a known atmospheric species but little is documented about its overall cycle within the atmosphere. There are many known sources of methanol, including seeds, fruits, leaf tissue of flowering plants, plant decay, biomass burning, chemical reactions in the atmosphere and ocean and from anthropogenic activities as noted in reference[5] and references therein. Methanol is thought to be one of the more significant organic compounds in the atmosphere, for being a substantial sink for hydroxyl radicals and also having a high annual carbon turnover.[5] Despite this information, the sources of atmospheric methanol outweigh the known sinks. This leaves a gap in the knowledge of atmospheric methanol and its overall cycle, providing an opportunity for further research. Therefore, as halogens and methanol both exist in the atmosphere, and having both cycles yet to be fully determined, this project aims to address deficiencies in our understanding of the complex reactions in the atmosphere.

1.3 Current Literature

There has been much experimental and theoretical effort expended towards elucidating the structures and energetic properties of anion - molecule complexes. High Pressure Mass Spectrometry (HPMS) was one of the first techniques used to study the solvation of ions in the gas phase.[6] Used by many groups, including Hiraoka and Yamabe,[7] HPMS determines the thermodynamic properties of ion - molecule clusters, such as enthalpies, entropies and the Gibbs free energies.

For studying the structural properties of ions, spectroscopy has an important role to play, and indeed vibrational predissociation spectroscopy is useful,[6] providing high resolution intermolecular - vibrational spectra of the clusters. As an example, work has been done on caesium ions solvated in methanol and ammonia using vibrational spectroscopy by Draves et al.,[8] finding the first solvation shell consisted of ten methanol molecules, as determined from analysis of the spectra. Monte Carlo simulations confirmed these results, suggesting a significant role for hydrogen bonding in the clusters formed by more than ten methanol molecules.[8] Photoelectron spectroscopy (PES) has been used to study the electronic structure of clusters and is useful for detailing the ion - molecule interactions within the clusters.[6] A PES experiment will assist in identifying cluster binding, vertical detachment and electron stabilisation energies upon increased cluster size. For example, the group of Markovich[6] used PES to study Cl^-, Br^- and I^- solvated in water clusters and were able to find the number of water molecules needed to form the first solvation shell, and the binding and stabilisation energies. Ab initio calculations were performed to confirm these results, with often the synergistic approach propelling forward developments in both experiment and theory.

The Wild group has taken advantage of PES coupled with a Time of Flight Mass Spectrometer (TOF - MS) to study various halide - molecule complexes. Recent studies include the halide - nitrogen,[9] halide - acetone[10] and halide - ethylene clusters.[11] In combination with high level theoretical calculations, the results of the experiments confirm the usefulness and importance of PES.

In regards to halide - methanol specific clusters, there has been a range of studies completed. Hiraoka and Yamabe[7] have performed HPMS experiments on the halide - methanol clusters, finding the first solvation shell for X^- ... methanol clusters, where X^- = F^-, Cl^-, Br^- and I^-. Hiraoka and Yamabe investigated the energetics of these clusters, finding enthalpies, entropies and Gibbs free energies of the clusters, studying the increases or decreases as additional methanol molecules were added. They also performed ab initio calculations to determine cluster composition for $X^- \ldots (MeOH)_n$, where n = 1-4. The Neumark group have used PES to investigate the charge transfer of iodide - methanol clusters from the anion to the methanol,[12] studying the vertical detachment energy and form of the spectra to determine the relaxation pathways. Mak and Peslherbe similarly looked at the charge transfer for an iodide - methanol system,[13] however from a computational perspective, elucidating similar results. Several groups have used infra - red predissociation spectroscopy to study halide - methanol solvation, with ab initio calculations to back up experiment, including Robertson et al.,[14] Corbett et al.[15] and Cabarcos et al..[16] In this work, the halides were shown to undergo surface solvation, whereby the halide adheres to the surface of a cluster of methanol molecules, and by studying the O−H stretching frequencies, an idea of how the cluster structures changed with increasing methanol molecules was formed. Using theoretical methods, Ayala et al. have studied the micro - solvation of the bromide anion in methanol at the DFT (B3LYP) level, focusing on solvent - solvent and solvent - ion interactions.[17] They found that unlike halide - acetonitrile clusters where an interior solvation was favoured, halide - methanol clusters consisted of both ion - solvent and solvent - solvent interactions, leading to a surface solvation.

Despite this extensive research, to date TOF-MS/PES has not been used to study chloride - methanol and bromide - methanol clusters to determine optimised structure and important structural energies, nor has a single iodide - methanol cluster interaction been investigated by this method. This project aims to rectify this.

1.4 Experimental Theory

By addressing the halide - methanol clusters experimentally, it will be possible to develop an understanding of the potential energy surface of the neutral cluster. This will aid in detailing the reaction pathway for these clusters, improving our knowledge of their reactions in atmospheric conditions. Several experimental techniques will aid in this endeavour and these are described below.

1.4.1 Time of Flight

The theory behind Time of Flight (TOF) is important as the apparatus to be used makes use of this effect. With reference to the basic velocity and kinetic energy equations, the equation below is derived.

$$\epsilon_{\mathrm{KE}}=\frac{1}{2}\mathrm{m}(\frac{l}{t})^2 \tag{1.5}$$

A TOF apparatus measures the time (t) taken for a species to travel the length of a flight tube of fixed length (l). Therefore, as the time and length are known, kinetic energy and mass become the variables of focus. This leads to two types of TOF systems: fixed mass and fixed kinetic energy.

1.4.2 Time of Flight Mass Spectrometry

Time of Flight - Mass Spectrometry (TOF - MS) is a fixed kinetic energy system. That is, all anion species passing through the apparatus receive the same kinetic energy and will therefore travel at different speeds according to their mass. The heavier a species is, the slower it will travel, and a separation of species depending on mass will occur. This allows for isolation of anion clusters due to mass selection, prior to interrogation via other methods.

1.4.3 Time of Flight Photoelectron Spectroscopy

While TOF - MS uses a fixed kinetic energy scheme, Time of Flight Photoelectron Spectroscopy (TOF - PES) is a fixed mass TOF system, as PES studies electrons exclusively.

Using Equation 1.5, it is possible to determine the kinetic energy of the electrons. From here, the principle of the photoelectric effect is employed to provide the electron binding energy, i.e., the energy required to dislodge the electron from the molecule.

The photoelectric effect is the emission of an electron when a photon interacts with an atom, molecule or cluster.[18] If a photon interacts with the sample, and has sufficient energy for the electron to overcome its binding energy, the electron will be ejected. X - rays and ultraviolet radiation are common sources of photons, and correspond to electrons being ejected from the core and valence energy levels respectively.[18] This process is represented in the equation below,

$$\epsilon_{\mathrm{KE}}=\mathrm{h}\upsilon-\epsilon_{\mathrm{BE}} \tag{1.6}$$

where $\mathrm{h}\upsilon$ is the photon energy and ϵ_{BE} is the electron binding energy.

Therefore, as the photon energy introduced into the system is known, and the kinetic energy is measured from the time of flight, one can then determine the binding energy of the electron.

In addition to determining the binding energy of an electron, PES essentially probes the neutral potential energy surface, defining the neutral ... neutral interaction.[19] A potential energy surface describes the energy of a system, depending on the position of the atoms involved. An example potential energy surface is given in Figure 1.2, of the fictitious A ... B complex. In relation to this project, the values of importance are the electron affinity (EA) and the vertical detachment energy (VDE). The EA corresponds to a ground state to ground state transition and will show as the highest kinetic energy transition. The VDE is the most likely transition and follows the Franck-Condon principle, which states the most favourable transition will result in the smallest change in geometry, and will be seen as the strongest peak. Therefore, potential energy surfaces can be created from PES spectra, revealing information on the structure and energies of the neutral cluster, thereby allowing for determination of the important reaction pathways.

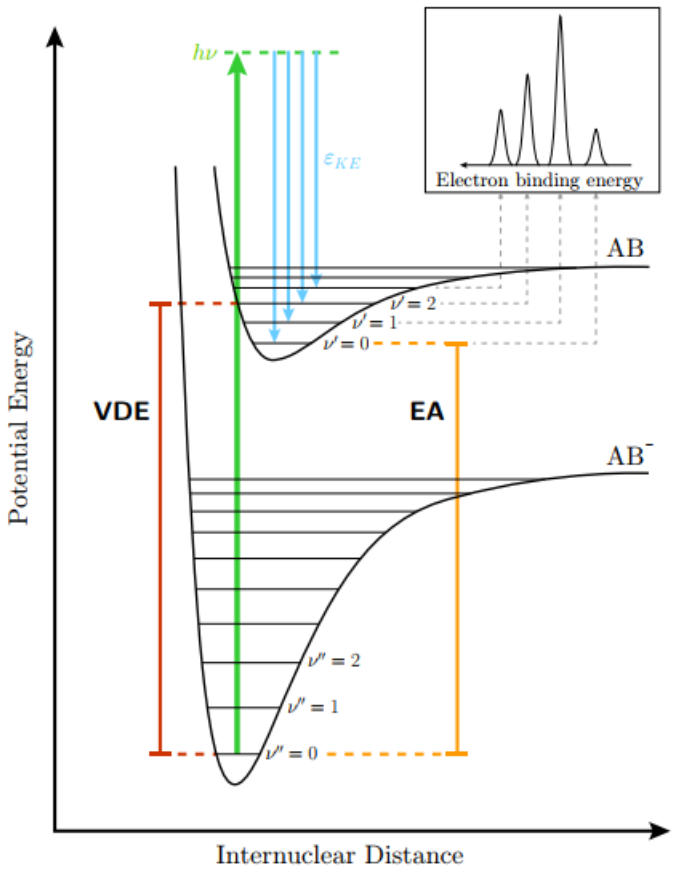

Figure 1.2: Schematic representation of the potential energy surface of the fictitious A . . . B complex [18]

1.5 Computational Theory

Interplay between computational and experimental results leads to a well - rounded and comprehensive study of ion - molecule clusters. Computational chemistry involves a series of calculations designed to solve the Schrödinger equation for a complete description of the system. [19] In doing so, the potential energy surface of the system can be probed, leading to values for optimised bond lengths and angles, the system's energy and vibrational frequencies. [20]

The time - independent Schrödinger equation only takes into account stationary states of the system. Wave functions represent these stationary states and have definite energies. These energies can be calculated using the time - independent Schrödinger equation by relating to

an appropriate Hamiltonian operator, which consists of kinetic and potential energy operators.[20]

Ab initio calculations are performed from first principles and provide solutions to the time - independent Schrodinger equation. The methods to be included are Hartree - Fock (HF), second order Mϕller-Plesset Perturbation Theory (MP2) and Coupled Cluster Theory (CC).

Many - electron atoms and molecular systems are too complicated for direct solutions of the Schrödinger equation.[21] Approximate solutions are found using methods with varying levels of approximation. One of the earliest methods is HF theory, which addresses the problem of the electron - electron interactions for many - electron systems by treating the interactions not as separate entities but as an average field of electron interaction. A drawback to the method is the problem of electron correlation not being taken into account, however post - HF methods provide solutions to this.

MP2 is one such post HF method which divides the Hamiltonian operator into two parts, an unperturbed Hamiltonian and a perturbation.[21] In doing so, it increases its applicability by accounting for up to (92.4 +/- 4.6) % of the electron correlation energy.[22] A disadvantage of MP2 is that for more accurate results one must increase the basis sets to higher levels of sophistication.[22]

Instead of splitting the Hamiltonian into unperturbed and perturbed like MP2, CC adds determinants to the wave function.[21] These determinants account for electronic correlation energies. While CC theory can allow for excitations to occur at single excitations, double excitations and so on, it most commonly stops at single and double. However, triple excitations can be approximated perturbatively, which is desirable as the accuracy increases greatly.[21] For this project, CCSD(T) will be the method of choice for CC theory, as it is the highest level of theory that will give the most accurate results in the available time.

Basis sets are the approximations of atomic orbitals, which are subsequently used to build molecular orbitals. For this project Dunning's[23–26] augmented correlated - consistent basis sets aug-cc-pVXZ, where X=D, T, Q, 5, are chosen. Aug stands for augmented and adds diffuse functions, which are needed as the ion - molecule clusters are loosely bound and these functions better describe the long range interactions.[24] Cc is correlation - consistent and allows for a basis set extrapolation to infinite basis set size by the addition of functions in shells, which is desired for producing more accurate energies for the prediction of the vertical detachment energy and electron affinity.[23] The pV denotes polarised valence, which refers to addition of mixing orbitals to allow the atomic orbitals to polarize.[23] D, T, Q, 5 are the increasing levels of basis set sophistication, standing for double, triple, quadruple and quintuple respectively. Additionally, for chlorine, the aug-cc-pV(X+d)Z basis sets will be used, as they have additional d-functions which improves the convergence.[26] For bromine and iodine, aug-cc-pVXZ-PP will be used, where the PP stands for pseudopotential, as it reduces computational time by using a pseudopotential which approximates the core electrons, and it also accounts for relativistic effects.[27]

1.6 Project aims

With the conspicuous lack of knowledge of halogen and methanol atmospheric chemistry, this project aims to fill this gap by determining possible reaction pathways involving these species. This will be accomplished by:

- Using a TOF-MS/PES apparatus to probe the structure and properties of gas phase halide (Cl^-, Br^- and I^-) and methanol clusters.
- Using computational chemistry to complement and extend the experimental results.

Information on the neutral states of the clusters will be obtained from the photoelectron spectra, such as the cluster binding energy, stabilisation energy and the vertical detachment energy. Ab initio calculations performed will complement the experimental results acquired. By completing these steps, greater insight into the interactions between halogens and methanol will be obtained.

Chapter 2

Methods

This chapter details the methods undertaken for experimental and theoretical analysis. This will include an overview of the TOF-MS/PES apparatus used during experiments, spectral analysis, computational methods and computational data analysis. The rationale behind the methods and any problems encountered are explained in this section.

2.1 Experimental Methods

The experimental portion of this project was performed using a custom built TOF-MS/PES apparatus based on a Wiley - McLaren[28] style mass spectrometer in the Wild lab, as seen in Figure 2.1. The workings of the apparatus and any troubleshooting are set out below.

2.1.1 Gas Mixture Creation

This first step in the experimental methods was the creation of the gas-phase anion clusters required for probing, using the gas mixing station as seen in Figure 2.2. There are three components to every gas mixture. Argon, the carrier gas, is brought into the gas mixture chamber through a teflon tube attached to a gas bottle, while the halide donor species (CCl_4, CH_2Br_2 and CH_3I) and the solvating species (methanol) enter into the gas mixture chamber by vials attached to the apparatus using their vapour pressure. There are several steps required for creating a gas mixture.

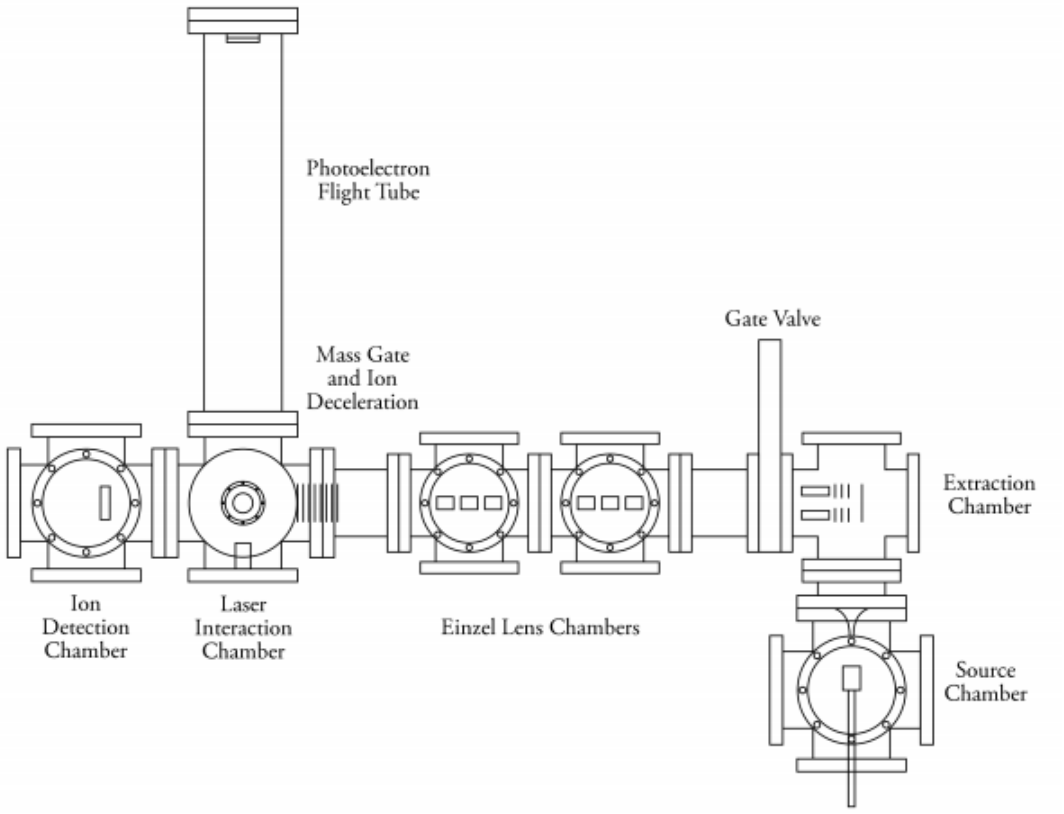

Figure 2.1: Top down view of TOF-MS/PES machine[29] (adapted from Ref. 29)

The previous gas mixture must be pumped out before a new gas mixture can be created. The chamber was pumped down using a rotary pump, with a liquid nitrogen trap added to increase efficiency. Argon was flushed through the chamber three times to encourage desorption of any traces of substances left from the previous gas mixture, and the chamber then pumped down to approximately 20-30 mTorr.

The halide donor species and methanol were then subjected to a freeze, pump, thaw cycle, which involved freezing the sample vials in liquid nitrogen, opening the vials so that any gases present were pumped away, closing the vials and then thawing the samples. This was repeated several times until all dissolved gases had been removed. Once this cycle had been completed, the halide donor species and methanol were then allowed into the chamber.

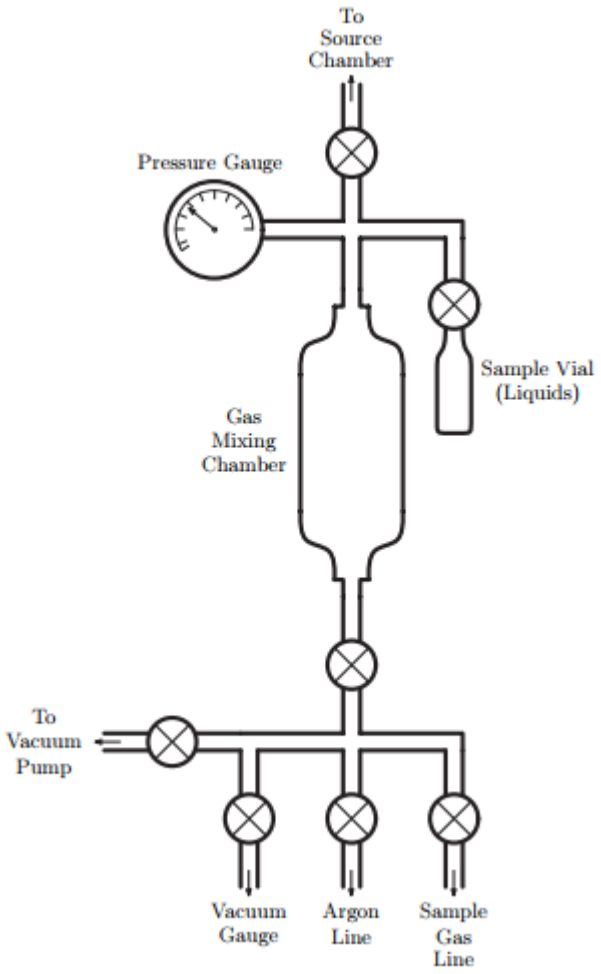

Figure 2.2: Gas mixing station schematic[18]

The process of allowing the halide donor species and the methanol into the gas mixture chamber is an important and crucial step. It is important that the ratio of the halide donor species to methanol is optimal for creating appropriate gas phase clusters. The first time the chloride - methanol cluster was created, a large amount of methanol was added, which led to nozzle instability and a poor amount of the cluster formed for probing. This problem was resolved with a new gas mixture creation, where the methanol was cooled using an ice - water bath, and the sample vial only opened for approximately thirty seconds instead of the few minutes as it was the first time. The CCl_4 was then opened for a few seconds, and a gas mixture with appropriate methanol to halide ratio was created, which became the standard creation procedure for following experiments. The chamber was then filled with argon to approximately 400 kPa and left to settle over night, where it was then ready for use the next day.

2.1.2 Source Chamber

As seen in Figure 2.2, the point of entry of the gas mixture into the TOF - MS/PES is the source chamber. The gas mixture enters the source chamber through a solenoid nozzle, which is pulsed at 10 Hz, where it undergoes a supersonic expansion. The purpose of a supersonic expansion is to narrow the range of velocities experienced by the molecules in the gas mixture, so that the spectroscopic resolution increases. A gas expansion requires energy, and as this supersonic expansion is occurring under vacuum, the energy source must be the gas molecules. This will result in a depopulation of the higher energy levels, producing a gas mixture with a high proportion of ground state molecules, which is essential for spectroscopic experiments.[19]

Current runs through a rhenium filament, leading to emission of electrons. The filament is then pulsed with -500 V, ejecting the electrons to then intersect with the supersonic gas expansion. This pulsed electron stream has several parameters that can be adjusted for optimisation, including current, width and timing of the pulse. A small Einzel lens is used to focus the electrons to optimise the intersection with the supersonic gas to improve cluster formation.

The intersection of the electrons and supersonic gas causes dissociative electron attachment,[30] which forms the negative ions and clusters. This process is outlined below in Equations 2.1 - 2.3.

$$\mathrm{Ar} + \mathrm{e^-_{fast}} \longrightarrow \mathrm{Ar^+} + \mathrm{e^-_{slow}} + \mathrm{e^-_{fast}} \tag{2.1}$$

$$\mathrm{e^-_{slow}} + \mathrm{CH_3I} \longrightarrow [\mathrm{CH_3I}]^* \longrightarrow \mathrm{CH_3} + \mathrm{I^-} \tag{2.2}$$

$$\mathrm{I^-} + \mathrm{CH_3OH} \longrightarrow \mathrm{I^-} \ldots \mathrm{CH_3OH} \tag{2.3}$$

The anion species formed, neutrals and cations then pass through a skimmer, designed to take the central portion of the gas expansion to create a beam with uniform velocity, and enter the extraction chamber.

2.1.3 Extraction Chamber

A series of TOF plates reside in the extraction chamber, designed to send the anions down the time of flight axis. This is accomplished by setting the voltage across one plate lower than that of the other plate, directing negatively charged species towards the plate with the lower voltage and ultimately, down the TOF axis. Neutrals are unaffected, while cations are sent in the opposite direction, as depicted in Figure 2.3.

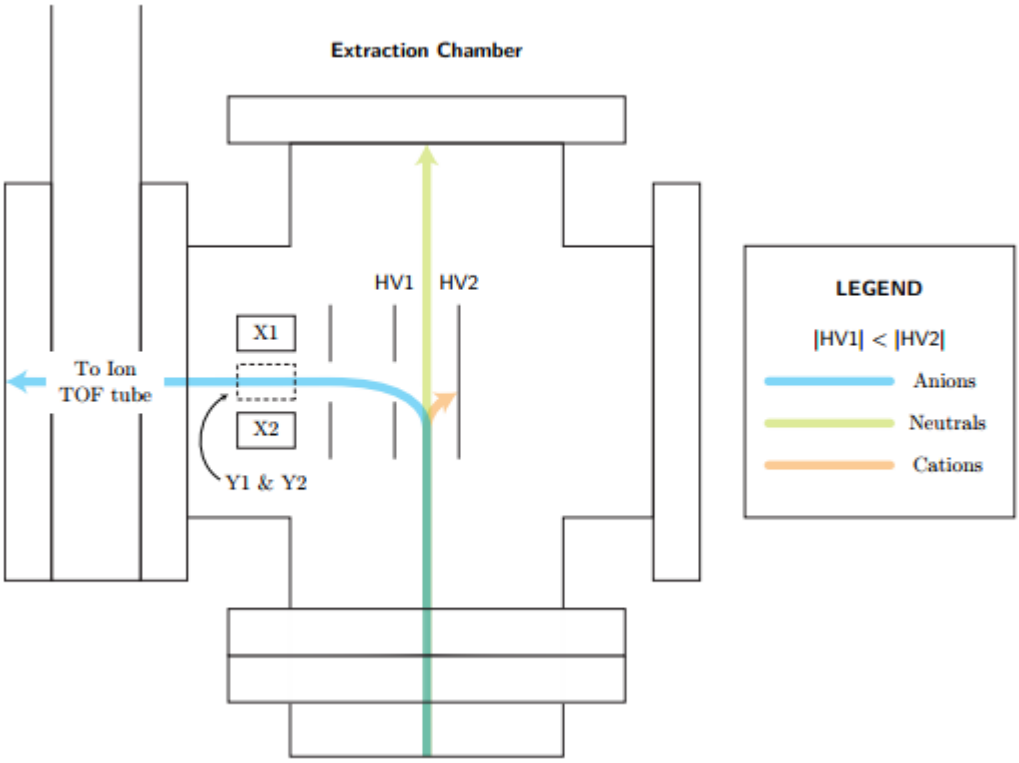

Figure 2.3: Ion deflection through TOF plate assembly[18], where HV1 and HV2 are the TOF plates and X1, X2, Y1, Y2 are deflection plates

The voltages applied to the TOF plates affect the speed at which the anions pass through the TOF axis. The values at which the plates were normally set were -1350 V and -1500 V, corresponding to HV2 and HV1 in Figure 2.3 respectively. Lower values resulted in poor ion signal and it is undesirable to have them set at higher voltages, which results in an increase in Doppler broadening and at higher voltages, the anion species have had less oppurtunity to spread out, so that in addition to the laser interacting with the species of interest, there may be noise from the laser interacting with other species.

2.1.4 Time of Flight Axis

The anion species exit the extraction chamber and enter the time of flight axis. A set of X-Y deflection plates steer the beam, as depicted in Figure 2.3. The X-Y plates are set at a voltage between -100 V and 100 V and steer the beam in the horizontal and vertical direction. Due to repulsion between the negative species in the beam, spreading will occur. To counteract this affect, two Einzel lenses are placed within the TOF axis to reduce the beam radius. An Einzel lens consists of three cylinders, where the outer two cylinders are at ground potential and the central cylinder is at a negative voltage, creating an electrical field. The anion species are repelled by the electrical field and therefore, the beam radius reduces. Another set of X-Y deflection plates are placed after the Einzel lenses, not depicted in Figure 2.1, for further steering of the beam path. It is important to optimise the Einzel lenses and X-Y deflection plates so that the anion species can travel from the extraction chamber to the ion detector and so that the beam path can intersect the laser in the laser interaction chamber at optimal conditions.

While conducting experiments, it was noted that the X-Y plates were being optimised at their extremes, -100 V and 100 V, which led to questioning their integrity. The apparatus was opened and it was found that a wire was directly in the beam pathway and had been affecting the traversal of the anion species. The wire was subsequently moved out of the beam pathway, the TOF axis cleaned, and the X-Y deflection plate optimisation improved a little.

After the anion beam passes through the second set of X-Y deflection plates, it enters the mass gate and ion decelerator region. The function of the mass gate is to allow only anions of a certain mass to charge ratio into the laser interaction chamber. This functions by holding the mass gate at a negative voltage and only switching to ground when the desired anion approaches. This then repels anions that arrive before and after the anion of interest, while allowing the anion of interest to pass through unaffected. This anion then enters the ion decelerator, whose function is to reduce the velocity of the anion beam. This is achieved by a series of positively charged plates electrically connected by resistors. The first plate has

a high positive voltage, and as the plates progress, they consistently become less positively charged due to the resistors. This positive attraction the anion experiences reduces the anion's velocity. The mass gate and ion decelerator were not used during the experiments where spectra are presented in the next Chapter.

At the end of the TOF axis sits the ion detector where mass spectra are recorded. As the anion species receive the same amount of kinetic energy along the TOF axis, they separate due to their mass and produce a mass spectrum. By looking at the mass spectrum, it is possible to identify the cluster of interest and once this has been determined, one can undertake the photoelectron experiments.

2.1.5 Laser Interaction Chamber and Photoelectron Flight Tube

Photoelectron experiments commence in the laser interaction chamber, where the cluster of interest, having been defined through mass spectrometry experiments, intersects with laser radiation. UV radiation at 266 nm (4.661 eV), which is the quadrupled output of a Nd:YAG (Neodynium:Yttrium Aluminium Garnate $Y_3Al_5O_{15}$) laser pulsed at 10 Hz, coincides with the arrival time of the cluster of interest, causing photodetachment, producing both electrons and the neutral form of the cluster of interest.

The electrons are directed down the photoelectron flight tube by a bottle-necked shaped magnetic field designed to capture the maximum amount of electrons.[18] A permanent magnet is generally used to create this field, however due to poor performance of the machine the permanent magnet was swapped out for an electromagnet part way through experiments. The electromagnet produced slightly better results, but not to the quality expected, so new permanent magnets were ordered and replaced the electromagnet. Due to the swap, two clusters had spectra recorded using the permanent magnet (I^-...methanol and Br^-...methanol) while the third (Cl^-...methanol) was recorded using the electromagnet. The electrons travel down the photoelectron flight tube towards the photelectron detector, where the spectra are recorded.

For the best results while performing photoelectron experiments, certain parameters need to be optimised. These include instruments mentioned above such as the X-Y deflection plates, the Einzel lenses and TOF plates, as well as the timing of key components, as shown in a schematic in Appendix B.

2.2 Experimental Data Analysis

The results acquired from experiment need to be converted into usable values. The following section outlines how the recorded TOF data was converted to m/z values and electron binding energy for use in the Results and Discussion section.

2.2.1 Mass Spectra

An oscilloscope was used to record the mass spectra, with 256 pulses of the nozzle averaged for each spectrum and saved to computer. The mass spectrum was then calibrated, first by identifying TOF for peaks of known mass, which were generally the bare halides as their peaks are large and have known isotopic splitting patterns. Mass of the known peaks were then plotted against TOF to create the calibration curve. Using the calibration curve coefficients, TOF is converted to m/z, and the mass of unknown peaks are determined by plotting m/z against intensity. Clusters of interest are then determined and parameters optimised for these, so that photoelectron experiments run optimally.

2.2.2 Photoelectron Spectra

As previously mentioned, the photoelectrons ejected travel down the photoelectron flight tube, arriving at a detector where each arrival is counted as a single event. A TOF analyser is used to record the number of arrivals in a series of time bins, the raw data corresponding to number of photoelectrons detected as a function of their TOF. For photoelectron data analysis three components are required; spectra of the cluster of interest, spectra of the bare halide, and background spectra. Three spectra of the cluster of interest and the associated background spectra are needed for averaging, while one bare anion spectrum is needed for

calibration.

The first step is to convert the bin number to TOF, using Equation 2.4.

$$((fstchan * 16) + (bin - 1) * 2))/(1E^9) \tag{2.4}$$

fstchan is the start delay and was 0 in the analysis done for this project. The bare halide can then be plotted against TOF and the $^2P_{3/2}$ and $^2P_{1/2}$ peaks determined, in terms of TOF. These values are then plotted against ϵ_{KE} to produce a linear plot, represented in Equation 2.5.

$$\epsilon_{KE} = m(\frac{1}{TOF^2}) + c \tag{2.5}$$

The kinetic energies of the halide peaks are known by taking the binding energies provided on NIST[31] and subtracting these values from the 4.661 eV provided by the laser, as shown previously in Equation 1.6.

m and c are then found through a linear regression analysis and an equation linking ϵ_{KE} to $1/TOF^2$ is found. TOF is then converted to ϵ_{KE}, which in turn can be converted to ϵ_{BE} by subtracting ϵ_{KE} from 4.661 eV. Photoelectron counts of the cluster spectra are averaged, their backgrounds averaged, and the background subtracted from the cluster spectra. A twenty point smooth is then applied to the data. The photoelectron spectrum can now be viewed as a function of ϵ_{BE}.

Finally, a Jacobi transform is applied, which involves multiplying the intensities by TOF^3. This transformation is needed as when the x-axis was converted from TOF to ϵ_{BE}, the transformation was non-linear. Hence, the y-axis has to undergo an appropriate transformation to show the correct intensity. These intensities can now be plotted against ϵ_{BE}, and the peak positions found. These peak positions correspond to the clusters' electron binding energies, and by performing a similar analysis on the bare halides and plotting them against ϵ_{BE}, the bare halide electron binding energies may also be found. Subtracting the bare halide electron binding energy from the cluster electron binding energy provides the E_{stab} value, in eV.

2.3 Computational Methods

Computational work was carried out using the Gaussian 09[32] program, using both the Wild group computers and the Pople super-computer facilities.

The first step in determining cluster structures was to generate one-dimensional (1-D) segments of the potential energy surface for analysis using the Gaussian 09 keyword Scan at the MP2/aug-cc-pVDZ level of theory. The Z-matrix shown in Table 2.1 was used for both the anion and neutral potential energy scans, where A6 was the variable of interest for the scan, and D6 changed by 5 degrees in each subsequent scan, so that the 1-D segments could add to a two-dimensional (2-D) scan to give a complete picture of the potential energy surface.

Table 2.1: Z-matrix for scanning the geometry to elucidate the potential energy surface, where X is a dummy atom

X							
X	1	1.00					
C	2	B1	1	A1			
O	2	B1	1	A1	3	D1	
H	3	B2	4	A2	1	D2	
H	3	B3	4	A3	5	D3	
H	3	B4	4	A4	5	D4	
H	4	B5	3	A5	5	D5	
Cl	2	B6	3	A6	5	D6	

Once the scans had been completed and possible minima determined, geometry optimisations were performed at MP2/aug-cc-pVDZ (pVDZ-PP for iodide) level of theory from different starting Z-matrices to confirm these minima. The results from these calculations were then optimised again at MP2/aug-cc-pVTZ (aug-cc-PV(T+d)Z level for Cl and aug-cc-pVTZ PP for Br and I, which is carried throughout the project and from now on basis sets will be referred to as AVXZ) level, then followed by an AVQZ optimisation and an AV5Z single point energy (SPE). The basis sets were downloaded from the EMSL[33] basis set exchange. The aim was to then optimise at the CCSD(T) level of theory. However time did not permit for this and instead SPE calculations were performed up to CCSD(T)/AVQZ level, using the

MP2/AVQZ optimised structures, for use in complete basis set (CBS) extrapolation, which will be explained in the next section.

A problem arose where one anion cluster minimum, which appeared in the scans, was not able to be optimised at the MP2 level. CCSD(T) calculations were then performed using the CFOUR[34] program and the structure was able to be optimised at the CCSD(T)/AVDZ level. Due to time constraints, it was not possible to optimise this at any higher level of theory, and as this level of theory is not a clear indication that this is a viable structure, this stationary point was omitted.

Vibrational frequency calculations were undertaken to confirm that the structures optimised were indeed minima. This was indicated by no imaginary frequencies (true minimum), one imaginary frequency (transition state) or multiple imaginary frequencies (higher order saddle point). Most of these calculations ran smoothly, with the exception of several MP2/AVQZ frequencies which needed the keyword freq=numer to run to completion. Freq=numer specifies that the second derivatives of the energy be computed numerically using analytically calculated first derivatives, as opposed to calculating the second derivative analytically.

2.4 Computational Data Analysis

After energy and frequency calculations were completed for optimised geometries, this data was analysed. Firstly a CBS extrapolation was completed for all halide-methanol anion and neutral complexes, along with the anion and neutral of the bare halogens and lastly bare methanol, to determine the convergent energies. An MP2 CBS extrapolation, between MP2/AVQZ and MP2/AV5Z, was first undertaken, using single point energies calculated for a MP2/AVQZ optimized structure.

To find the CBS energy $E_{total}^{(\infty)}$, two components are needed: the Hartree-Fock energy E_{HF} and the correlation energy E_{corr}. These are extrapolated separately and then summed to give the final energy, as shown in Equation 2.6.

$$E_{total}^{(\infty)} = E_{HF}^{(\infty)} + E_{corr}^{(\infty)} \tag{2.6}$$

$E_{HF}^{(\infty)}$ is calculated using Equation 2.7.[35]

$$E_{HF}^{(\infty)} = E_{HF}(L+1) + \frac{E_{HF}(L+1) - E_{HF}(L)}{\frac{(L+1)exp(9(\sqrt{L+1} - \sqrt{L}))}{L+2} - 1} \tag{2.7}$$

Where $E_{HF}(L)$ and $E_{HF}(L+1)$ correspond to calculated HF energies at AVQZ and AV5Z respectively. E_{corr} is calculated in a similar way.

$$E_{corr}^{(\infty)} = E_{corr}(L+1) + \frac{E_{corr}(L+1) - E_{corr}(L)}{c-1} \tag{2.8}$$

$$c = \frac{(L+1)^{\alpha}}{L} \tag{2.9}$$

Where α is a constant dependent on the level of theory, in this case α=3.[36]

CCSD(T) extrapolations were done in a similar way, using a AVTZ/AVQZ extrapolation, except Equation 2.6 now becomes Equation 2.10.

$$E_{total}^{(\infty)} = E_{HF}^{(\infty)} + E_{corr(CCSD)}^{(\infty)} + E_{corr(T)}^{(\infty)} \tag{2.10}$$

Both $E_{corr}^{(\infty)}$ are calculated using Equations 2.8 and 2.9, while $E_{HF}^{(\infty)}$ is calculated using Equations 2.11 and 2.12.[37]

$$E_{HF}^{(\infty)} = E_{HF}(L+1) + \frac{E_{HF}(L+1) - E_{HF}(L)}{c-1} \tag{2.11}$$

$$c = \frac{(L+1)^{\alpha}}{L} \tag{2.12}$$

For this extrapolation, the HF and CCSD contributions are extrapolated from the AVTZ/AVQZ basis sets, while the (T) contribution is from the AVDZ/AVTZ basis sets. The α value is 5 for HF calculations, 3.22 for CCSD calculations and 3.22 for (T) calculations.[37]

Once the CBS extrapolation is completed, values of interest are calculated. These include the dissociation energy (D_0), the electron affinity (EA), the vertical detachment energy (VDE) and the stabilisation energy (E_{stab}). D_0 is the difference between the energy of the cluster and the sum of the energies of methanol and the bare halogen. EA is the difference in minimum energies of the anion and neutral cluster. VDE is the difference between the anion cluster's energy and the energy of a neutral cluster with the same geometry, as seen in Figure 1.2. E_{stab} is the difference in D_0 energies for the anion and neutral clusters.

Chapter 3

Results and Discussion

This section comprises results obtained from mass spectra, photoelectron spectra, and the geometries and energies calculated. Experimental and computational results will be compared and a comparison to literature will be given.

3.1 Experimental Results

3.1.1 Mass Spectra

CH_3I, MeOH and Ar was the first gas mixture created and its mass spectrum is presented in Figure 3.1. This same gas mixture is used to produce the photoelectron spectrum of I^-...methanol, which is presented in the next section. The bare halide was easily identified by its high intensity and after some educated guesses as to which was the I^-...argon peak, an initial calibration curve was plotted using the I^- (m/z value 126.9) and I^- ...argon (m/z value 166.8) peaks. The calibration was applied to the spectrum and the I^-...methanol peak was determined to lie at a m/z value of 159.1. Other notable peaks are I^- ...$(MeOH)_2$ and I^-...CH_3I at m/z values of 191.1 and 268.8 respectively.

The second gas mixture created was that of CH_2Br_2, MeOH and Ar and its mass spectrum is shown in Figure 3.2. Once again, the intensity of the bare halide makes it easy to identify, along with its recognisable isotopic splitting pattern. The bare bromide was therefore used

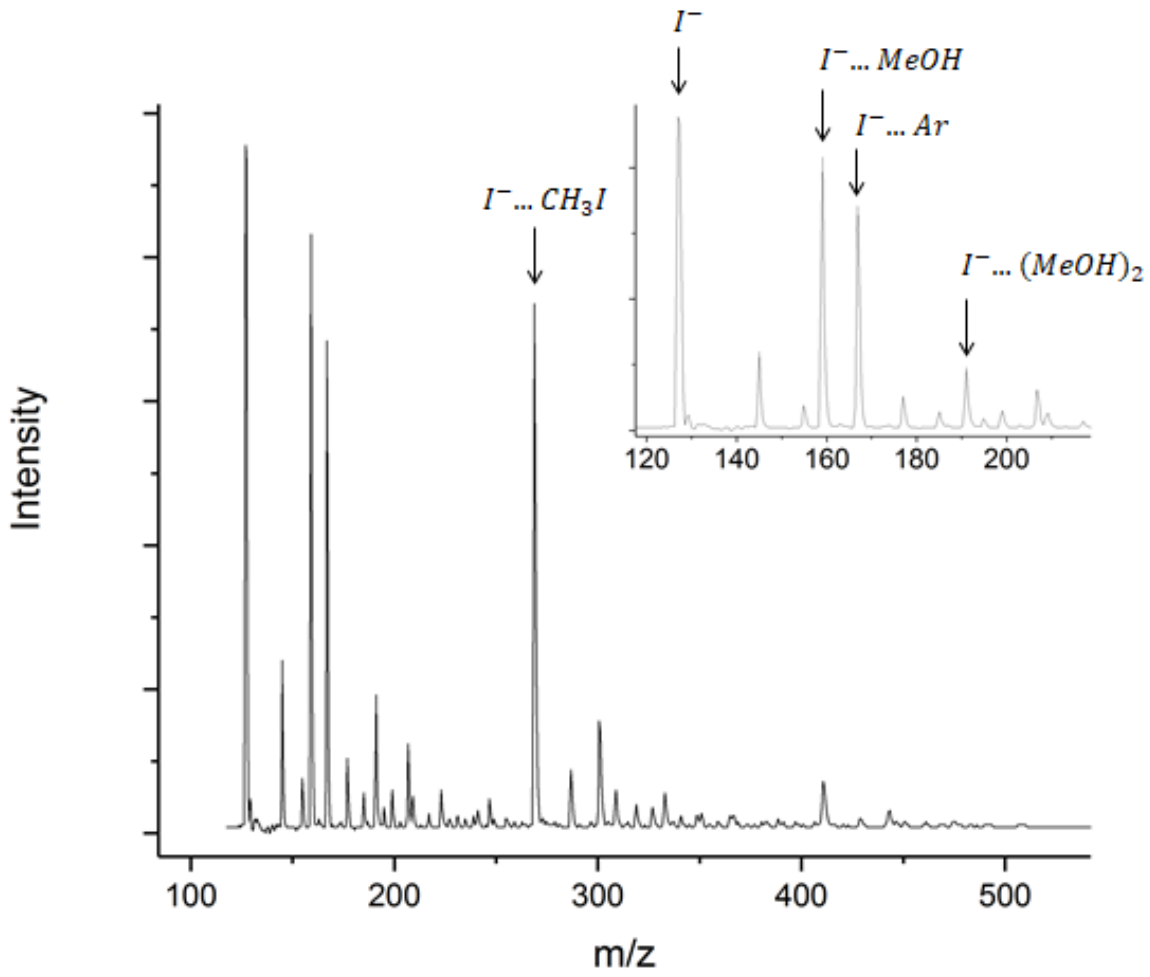

Figure 3.1: A mass spectrum of the CH_3I, MeOH and Ar gas mixture

initially to calibrate the spectrum, with the bromide peaks found to occur at m/z values of 78.9 and 80.9. The high intensity of the bare bromide compared to the cluster suggests that these conditions aren't favourable for cluster formation, or that parameters were optimised for the bare bromide instead of the Br^-... methanol cluster. From here, the Br^-... methanol peaks were determined to be 111.0 and 112.9 m/z respectively. Other notable peak positions include m/z values of 96.9/98.9 and 118.9/120.9, corresponding to Br^-... H_2O and Br^-... argon respectively.

Finally, Figure 3.3 shows the mass spectrum for the CCl_4, MeOH and Ar gas mixture, the last gas mixture created. The known splitting pattern of chlorine and its high intensity allowed for its peaks to be identified (at m/z values of 35.0 and 37.0) and used for calibration. The Cl^-

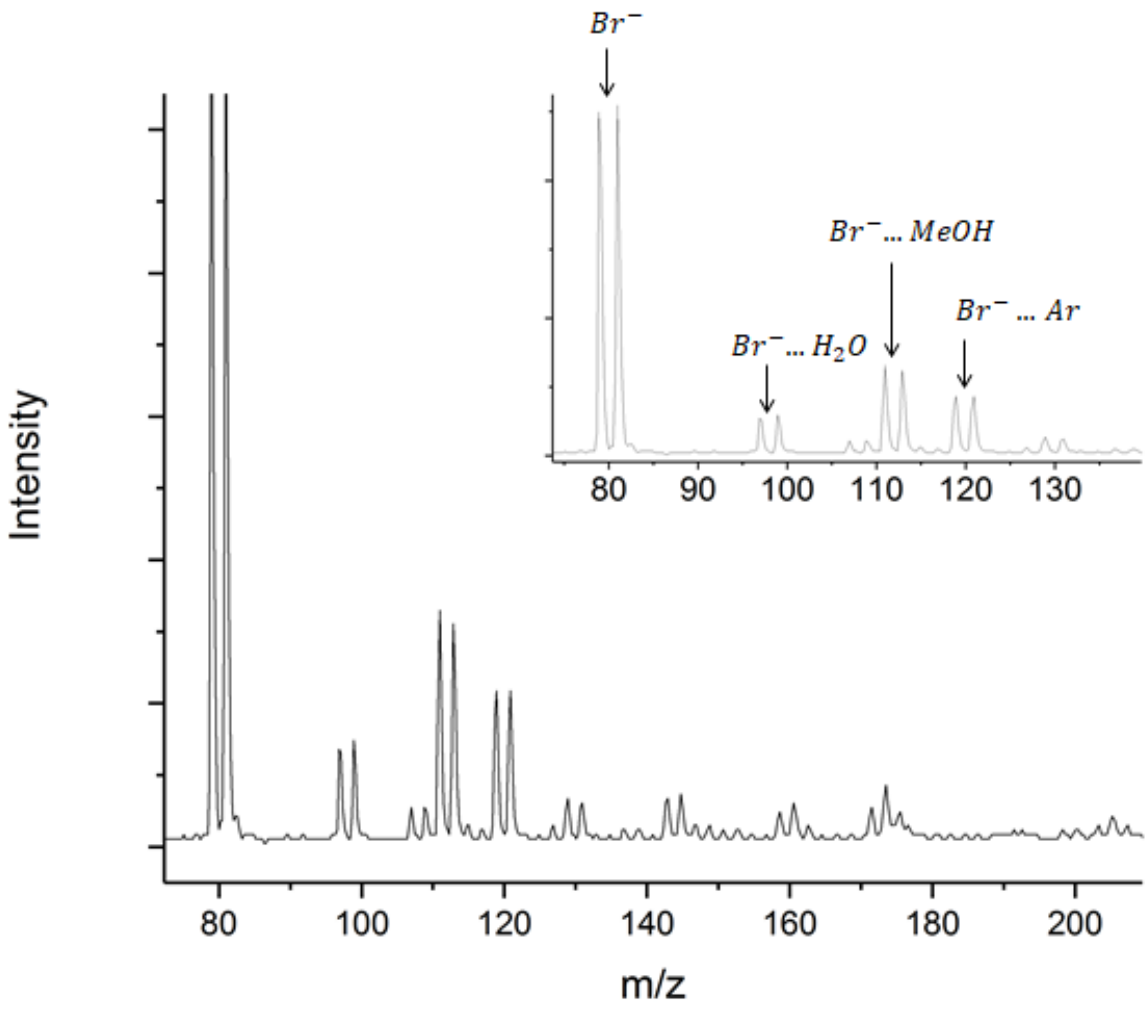

Figure 3.2: A mass spectrum of the CH_2Br_2, MeOH and Ar gas mixture

. . . methanol cluster peaks were then calculated to be 67.0 and 74.9 m/z. Once again, the intensity for the bare halide is much larger than the cluster, suggesting that conditions may be optimal for the bare halide rather than the cluster. Photoelectron spectra were still able to be taken of the Cl^- . . . methanol cluster despite this. Other peaks of interest include 74.9/77.0 and 99.0/101.0 m/z, corresponding to $Cl^-\ldots Ar$ and $Cl^-\ldots (MeOH)_2$, respectively.

After the identities of the clusters have been determined through mass spectrometry, photoelectron spectra were taken.

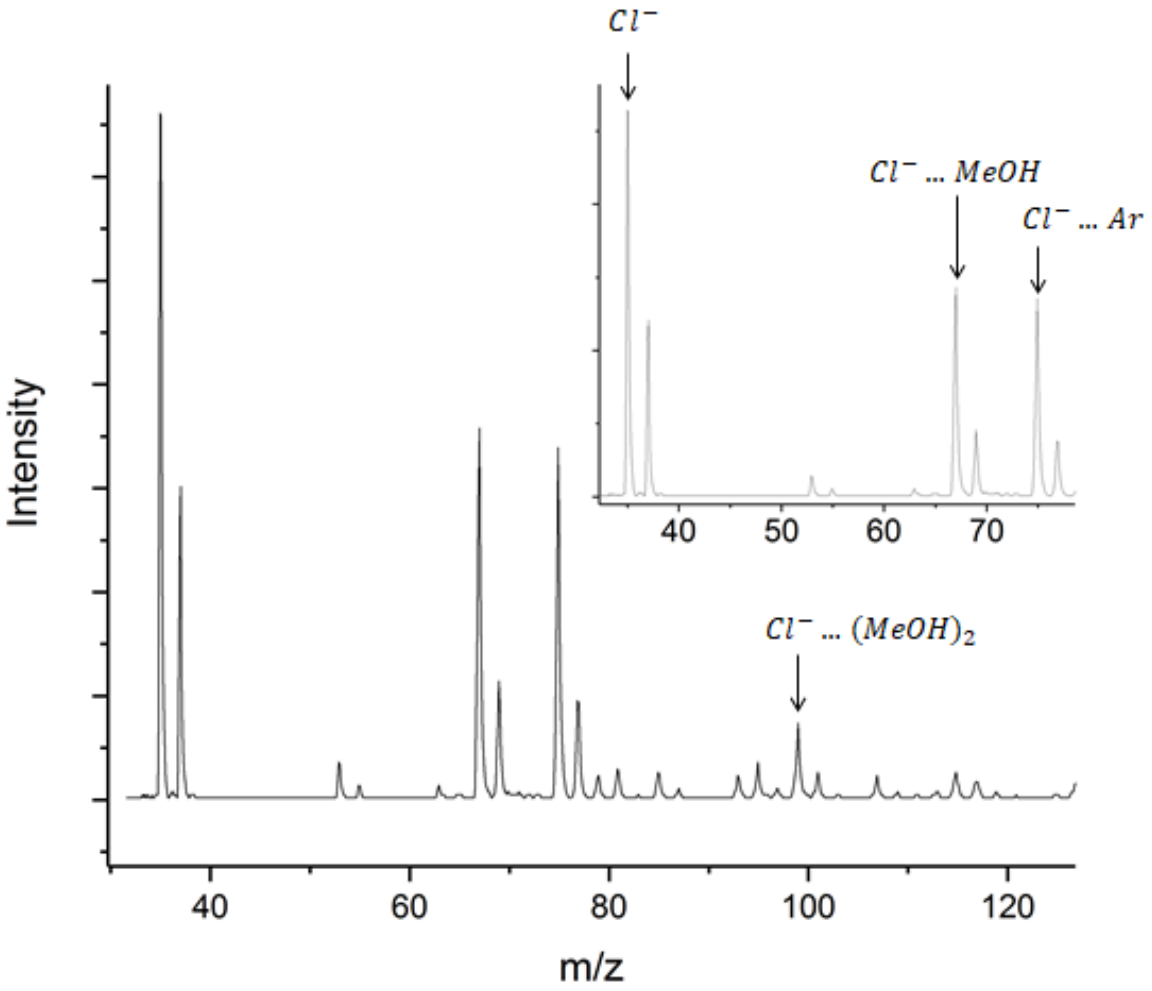

Figure 3.3: A mass spectrum of the CCl_4, MeOH and Ar gas mixture

3.1.2 Photoelectron Spectra

As previously mentioned, gas mixtures containing argon, methanol and a solvating species (either CCl_4, CH_3I or CH_2Br_2) were delivered into the apparatus and after mass spectra were produced, species of interest were identified and photoelectron spectra were taken. In particular, photoelectron spectra of I^-...methanol, Br^-...methanol and Cl^-...methanol were recorded and their experimental electron binding energies determined. Table 3.1 summarizes the experimentally determined electron binding energies of each cluster and its associated bare halide, in conjunction with each resulting E_{stab}, which is the difference in electron binding energies between the bare halide and complex.

Table 3.1: Experimentally determined electron binding energies and E_{stab} values for the halide-methanol clusters (eV), where the electron binding energies are determined from photoelectron experiments. The values in parenthesis represent uncertainty in the peak position, as determined by full width at half the maximum height

	Cl^-	Br^-		I^-	
	$^2P_{3/2}$	$^2P_{3/2}$	$^2P_{1/2}$	$^2P_{3/2}$	$^2P_{1/2}$
Halide	3.62(4)	3.36(15)	3.82(14)	3.08(17)	4.02(9)
Halide - methanol	4.58(7)	4.00(11)	4.38(4)	3.62(12)	4.53(3)
E_{stab}	0.96(11)	0.64(26)	0.57(28)	0.55(29)	0.51(12)

Looking at Table 3.1, a pattern is observed that as the halide size increases, the E_{stab} decreases, meaning the electron becomes less stabilised by the complex. This corresponds to a greater attraction for the smaller halide. The positive E_{stab} values also indicate that the clustering provides a stabilising effect for the electron attached to the halide. The E_{stab} values will be compared to the computationally determined difference of the dissociation energies (D_0) between the anion and neutral clusters in the computational results section.

As for the mass spectra, the first photoelectron spectrum taken was that of the I^-...methanol complex, and is presented in Figure 3.4. There is a clear splitting of the two peaks, corresponding to the transitions to $^2P_{3/2}$ and $^2P_{1/2}$ states of the halogen, with some noise between the two peaks. The $^2P_{1/2}$ peak is not as smooth as the $^2P_{3/2}$, as the Jacobi transform amplifies the noise at values close to the upper energy limit that the laser provides, which is also apparent by the bold line at the upper energy limit.

Figure 3.5 shows the recorded Br^-...methanol photoelectron spectrum. Once again, two peaks are clearly distinguishable, with slight overlapping, due to the resolving power of the spectrometer being only slighter above that of the separation between energy levels. The break in the smooth line before the $^2P_{3/2}$ peak is due to noise.

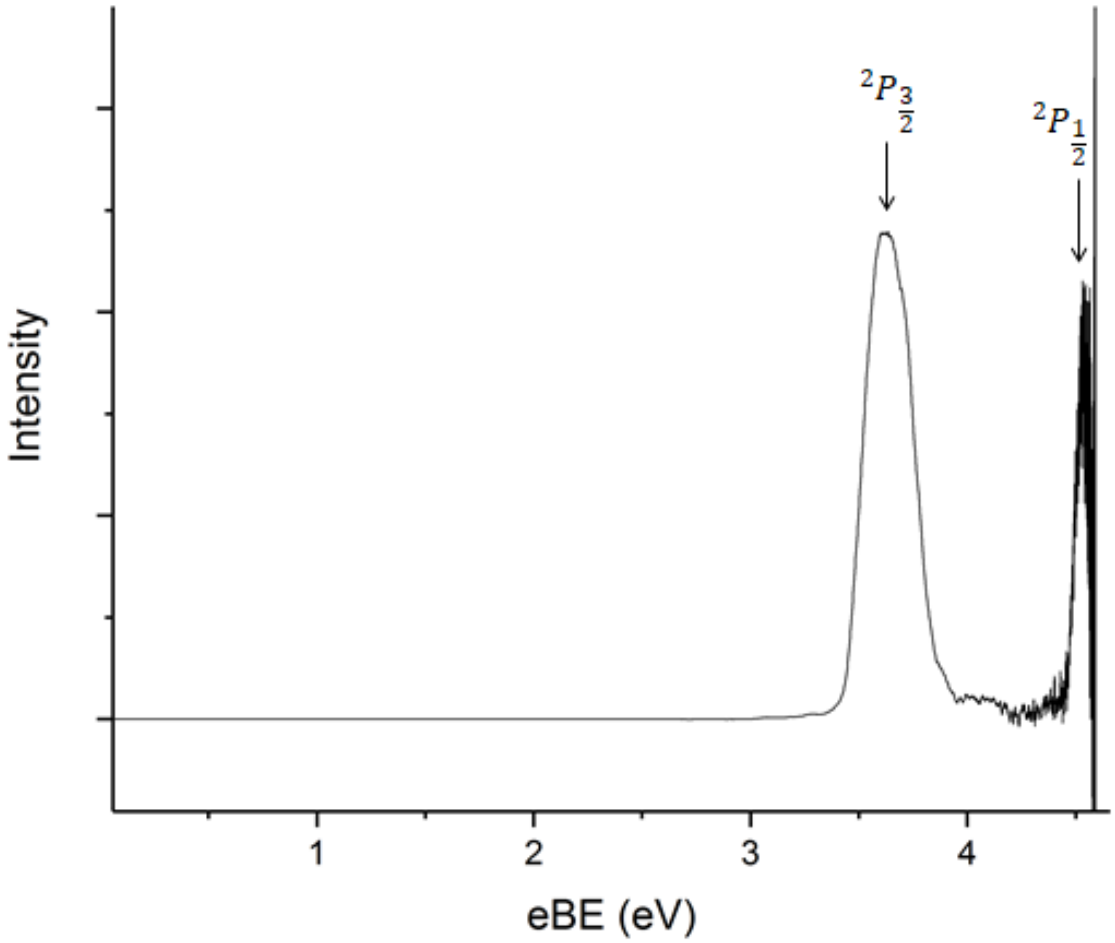

Figure 3.4: Photoelectron spectrum of the I^-...methanol complex

Finally, the Cl^-...methanol photoelectron spectrum is given in Figure 3.6. Unlike the other two spectra, only one peak is visible. This is due to the resolution of the spectrometer not being great enough to distinguish between the $^2P_{3/2}$ and $^2P_{1/2}$ energy levels. While this was the spectrum recorded, it is unreliable compared to the other two spectra for two reasons. Firstly, problems with the apparatus occurred at the time this spectrum was recorded, mainly drifting of the peaks throughout the day, leading to the permanent magnet being swapped for the electromagnet. This resulted in spectra with poor signal to noise being produced. Secondly, problems occurred during calibration of the photoelectron spectrum, as unlike with iodide and bromide where there are two peaks available for calibration, chloride only provided one peak. To calibrate the spectrum, bromide and iodide peaks from days close to when this

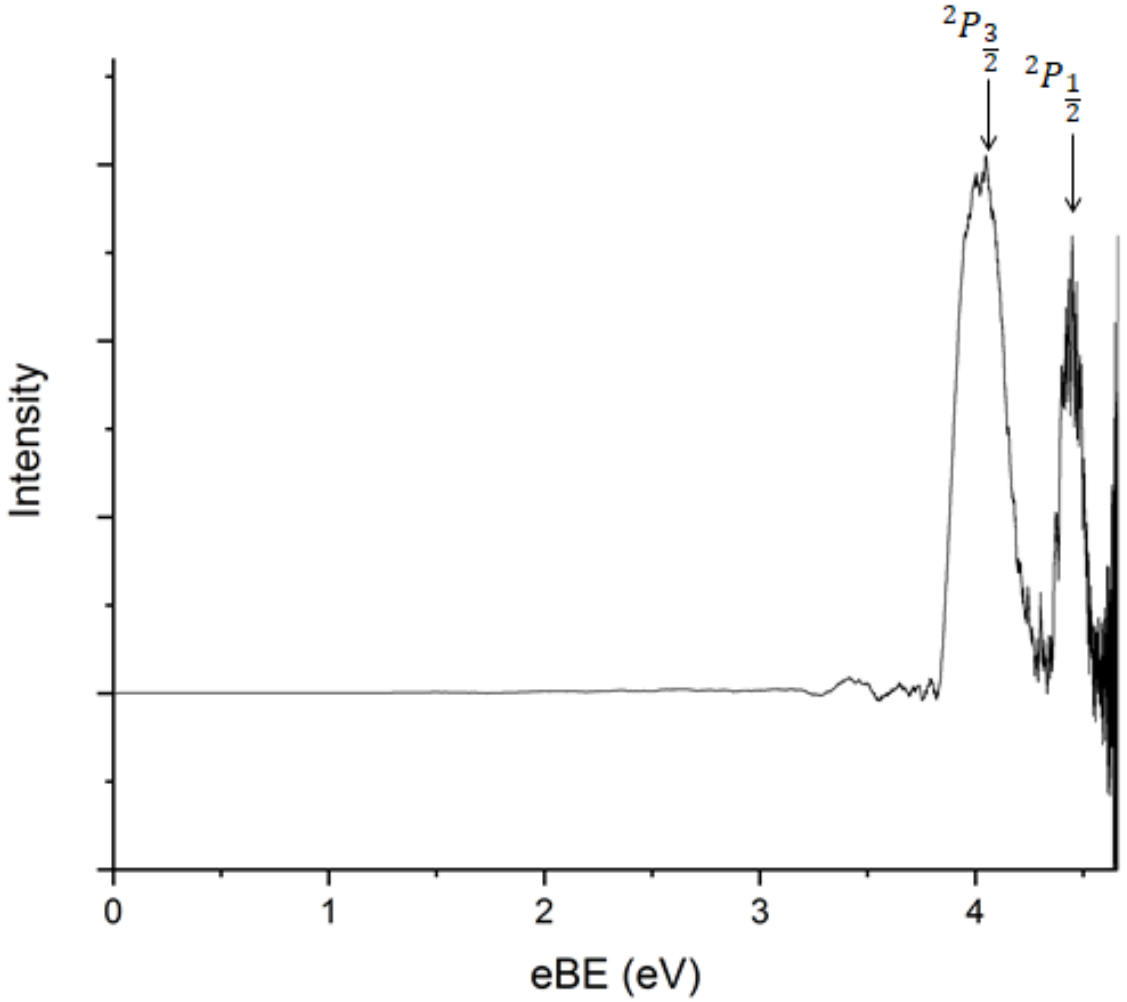

Figure 3.5: Photoelectron spectrum of the Br^-... methanol complex

spectrum was recorded had to be used, which resulted in a linear regression with Pearson's coefficient of 0.97. These two factors have resulted in an unreliable spectrum.

A limitation of experimental work is that structures can not be elucidated and this is an avenue where-by computational work can complement experimental work, as outlined in the next section.

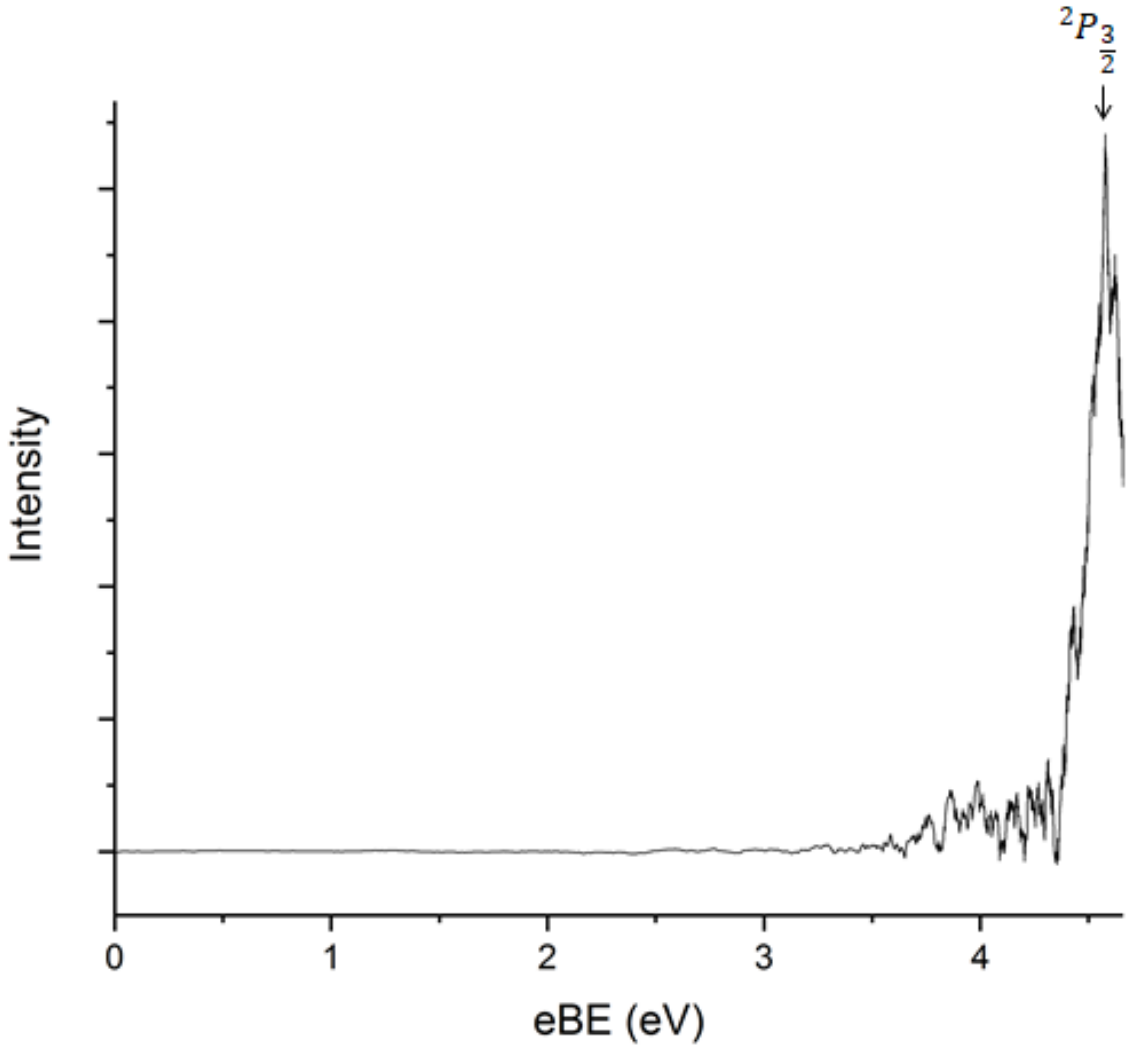

Figure 3.6: Photoelectron spectrum of the Cl^-... methanol complex

3.2 Computational Results

All halide-methanol and halogen-methanol complexes were optimised at the MP2/AVQZ level of theory, with single point energy calculations completed up to MP2/AV5Z and CCSD(T)/AVQZ. In addition to the determination of optimised geometries and vibrational frequencies, values such as the EA and VDE were calculated, as presented in this chapter.

For all images of structures shown, a green atom represents Cl, a brown atom represents Br and a purple atom represents I.

3.2.1 One Dimensional (1-D) Potential Energy Scans

As mentioned in the Methods section, a series of 1-D scans of the halide around methanol were conducted in order to create a 2-D potential energy surface, using the Z-matrix provided in Table 2.1, at the MP2/AVDZ level of theory. The scans completed were rigid 1-D scans, whereby the methanol was not able to optimise its geometry at each point. From these scans, possible anion stationary points were elucidated from the wells within the scans. A scan of interest is shown in Figure 3.7, with the corresponding structures presented in Figure 3.8.

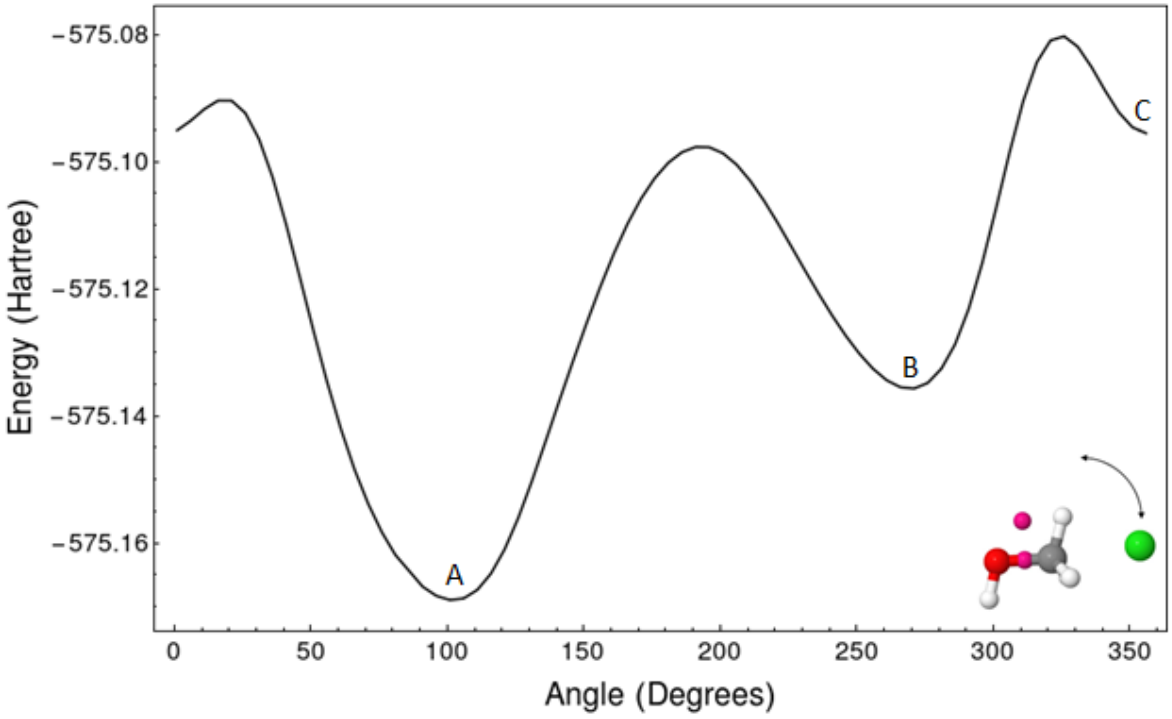

Figure 3.7: Potential energy surface scan of the Cl^- ... methanol complex, at the MP2/AVDZ level of theory, where the pink atoms represent dummy atoms

The geometry for well A was optimised, then verified with a frequency analysis, and found to be a minimum with the halide associated with the O-H bond of the methanol. The geometry for well B underwent the same process but unfortunately was not able to be optimised. Another scan was completed in the plane perpendicular and it was found that while well B had been a minimum for this plane, it was not in fact a well for the second plane, and the halide preferred to sit where well A had suggested a minimum would be. The geometry for well

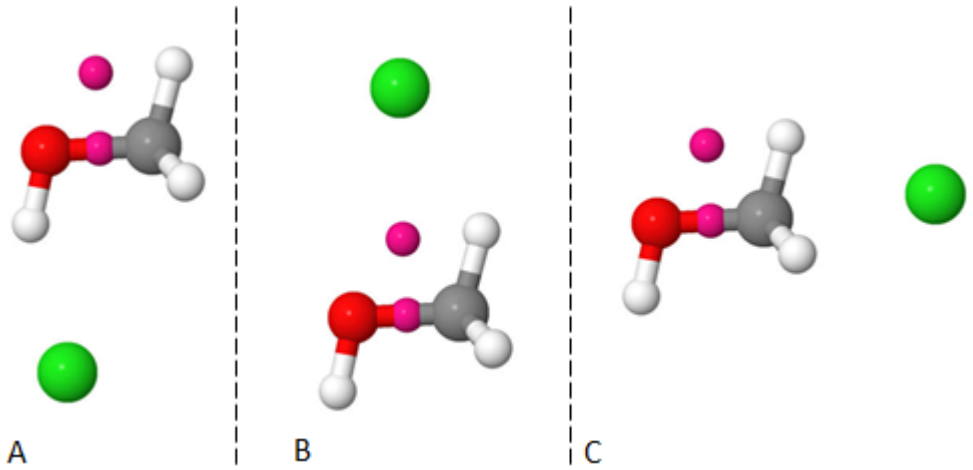

Figure 3.8: Structures corresponding to wells for the 1-D scan of the Cl^- ... methanol complex, at the MP2/AVDZ level of theory, where the pink atoms represent dummy atoms

C was not able to be optimised using the MP2 method but was optimised at CCSDT/AVDZ level of theory, with the halide sitting in the methyl pocket. Unfortunately, time did not permit for it to be optimised further, with problems occurring when a AVTZ optimisation was attempted, and this structure was omitted. Thus, for all anion halide-methanol clusters, one geometry was the subject of interest, an example given in Figure 3.9.

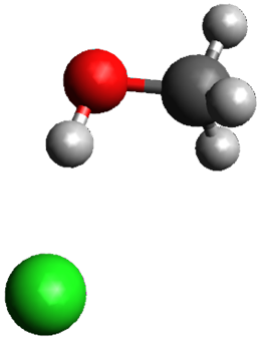

Figure 3.9: Cl^- ... methanol complex, at the MP2/AVDZ level of theory

Similarly, neutral optimised geometries were predicted from scans conducted of the halogen around methanol. Results from scans of interest are shown in Figure 3.10 and 3.11 and the geometries of the clusters they correspond to are shown in Figure 3.12.

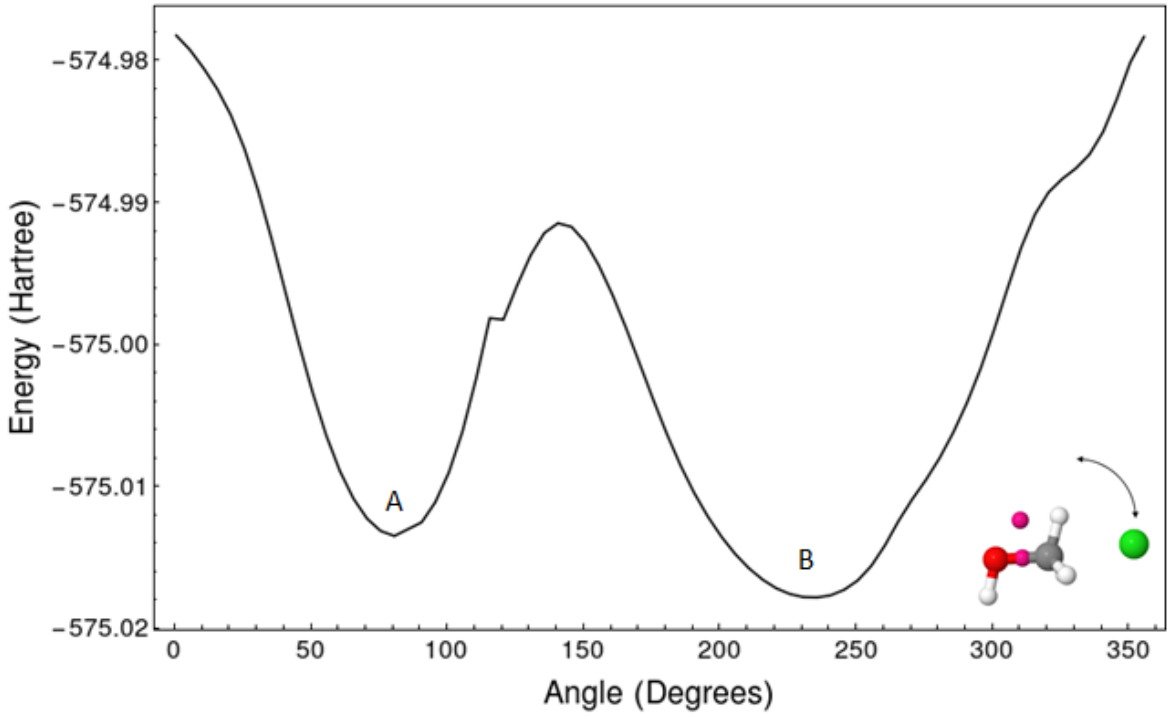

Figure 3.10: Potential energy surface scan of the Cl . . . methanol complex, at the MP2/AVDZ level of theory, where the pink atoms represent dummy atoms

Geometry optimisations were performed on the potential minima, with frequency calculations following, confirming that structures A, C and D from Figure 3.12 are in fact minima. However, when structure B was optimised it changed to structure C/D. Noting that this had appeared as a minimum in the scan, another scan was performed around the O-H bond, shown in Figure 3.13. This proves that while structure B had appeared as a minimum in one plane, it was not in fact a minimum in the other plane, and the halogen preferred to append to the oxygen as it does in structure C/D.

Examples of the two neutral structures determined are given below in Figure 3.14 and 3.15. For Figure 3.15, the halogen can occur on both sides of the oxygen, as this is a symmetrical structure.

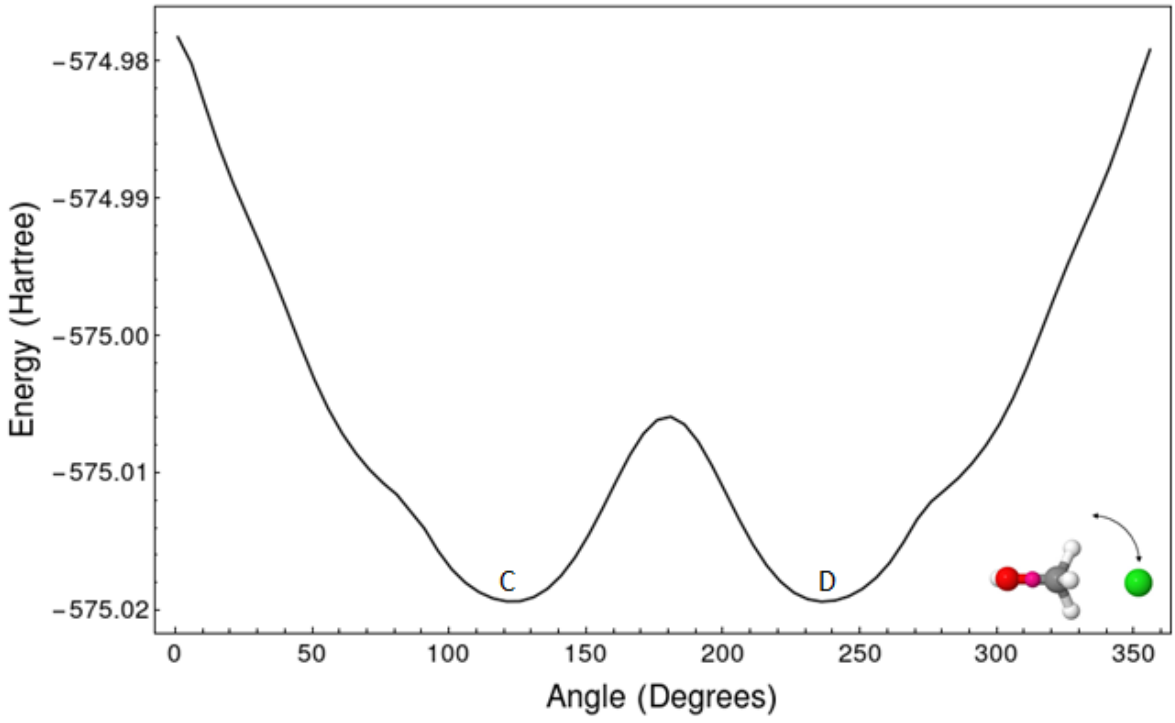

Figure 3.11: Potential energy surface scan of the Cl . . . methanol complex, at the MP2/AVDZ level of theory, where the pink atoms represent dummy atoms

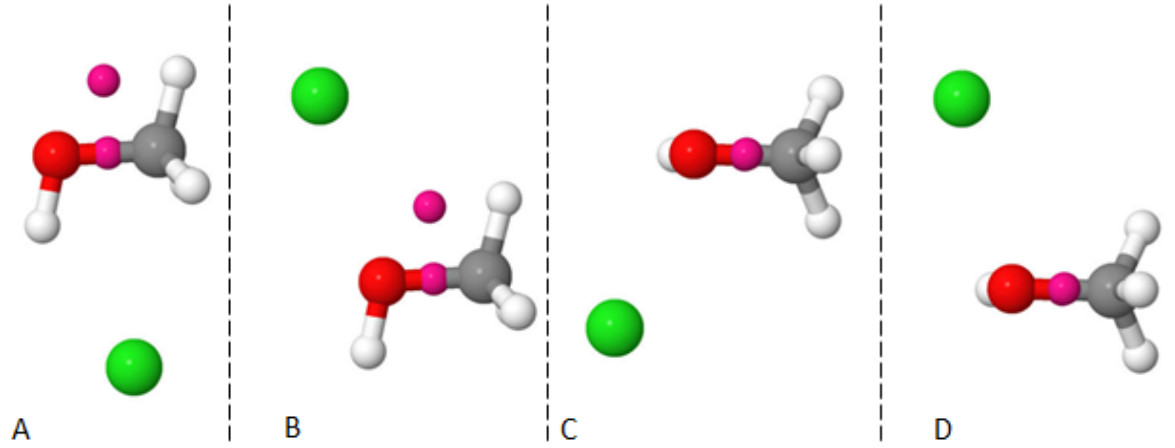

Figure 3.12: Structures corresponding to wells for 1-D scans of the Cl . . . methanol complex, at the MP2/AVDZ level of theory, where the pink atoms represent dummy atoms

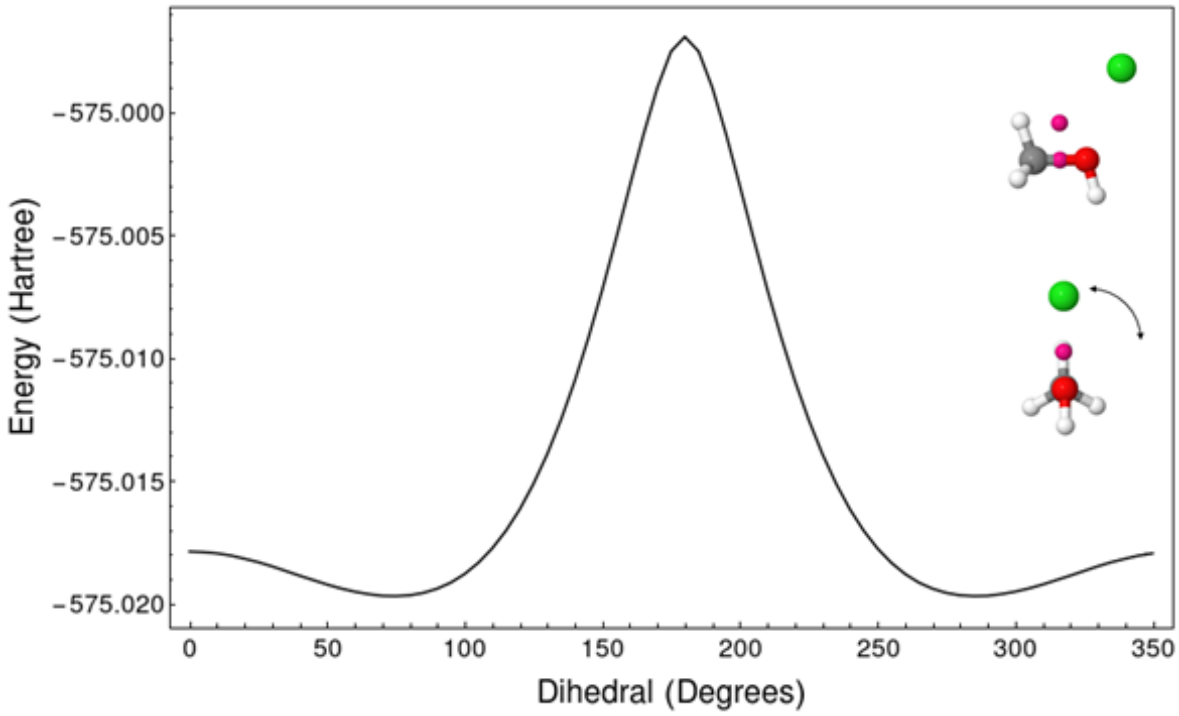

Figure 3.13: Potential energy surface scan of the Cl . . . methanol complex around the O-H bond, scanning through the dihedral, at the MP2/AVDZ level of theory, where the pink atoms represent dummy atoms

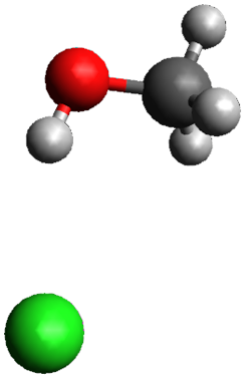

Figure 3.14: Cl . . . methanol optimised complex: Cl associated with O-H bond, at the MP2/AVDZ level of theory

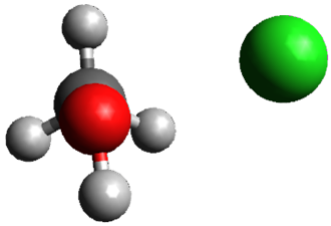

Figure 3.15: Cl . . . methanol optimised complex: Cl to right/left of O, out of plane, at the MP2/AVDZ level of theory

3.2.2 Chloride-Methanol Complexes

Figure 3.19 shows the optimised anion structure of Cl^- ... methanol, which has a C_s symmetry, with the chloride in plane with the O-H bond. The chloride sits 2.075 Å away from the hydrogen and makes a 167.1° angle with the appended hydrogen and oxygen. In regards to how the methanol structure changes with the addition of chloride, the O-H bond has increased from 0.959 Å to 0.991 Å.

The first Cl ... methanol neutral structure is shown in Figure 3.20, once again with a C_s symmetry as the chlorine lies in plane with the O-H bond. For this neutral complex, the chlorine sits at a distance of 2.615 Å from the hydrogen, while making a 157.6° angle with the hydrogen and oxygen. The second neutral structure is given in Figure 3.18, this time having a C_1 symmetry, as the chlorine lies either to the left or the right of the oxygen. The chlorine sits 2.450 Å from the oxygen and makes a 97.0° angle with the oxygen and appended hydrogen. A list of full geometries, for chloride and all other halide complexes, can be found in Appendix A.

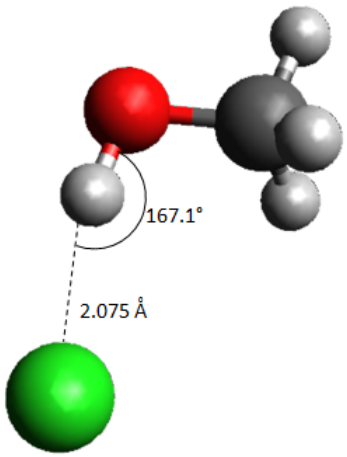

Figure 3.16: Cl^- ... methanol complex - C_s symmetry, optimised at the MP2/AVQZ level of theory

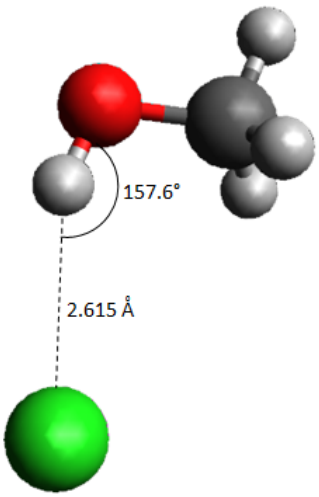

Figure 3.17: Cl ... methanol complex - C_s symmetry, optimised at the MP2/AVQZ level of theory

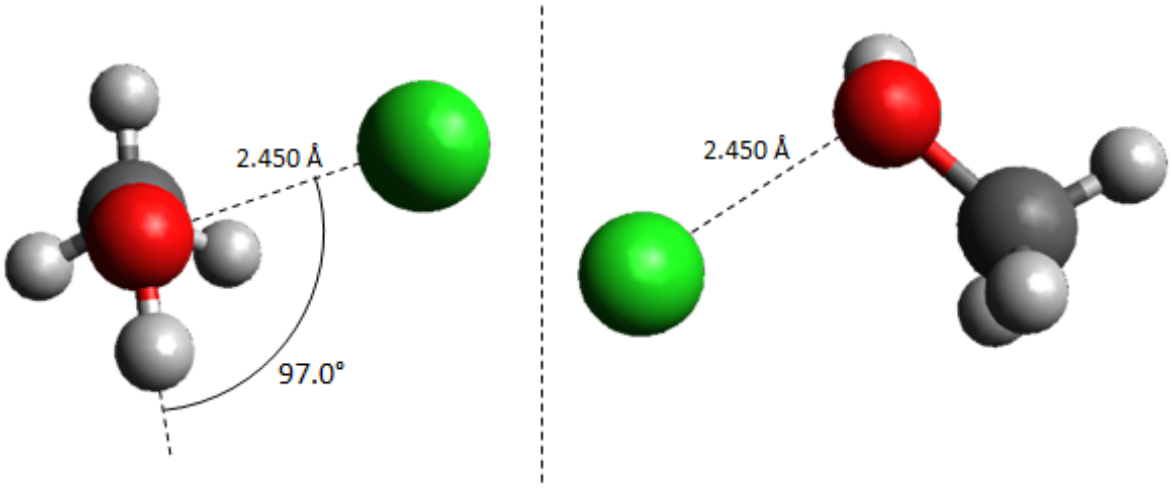

Figure 3.18: Cl . . . methanol complex - C_1 symmetry (L: Front view, R: Top view), optimised at the MP2/AVQZ level of theory

Electronic energies were calculated from both an MP2 and CCSD(T) extrapolation and are shown below in Table 3.2. The VDE, being the energy difference between an anion and a neutral at the anion's geometry, is listed alongside the anion energies, while EA, the difference in energy between an anion minimum geometry and neutral minimum geometry, is listed alongside the neutral energies. The binding energy taken from the photoelectron spectrum is listed under VDE, the reason behind this has been explained in the Introduction. Computational data will be represented this way for all halide-methanol complexes.

A comparison between MP2 and CCSD(T) values reveals the two CBS extrapolations calculated similar results, as is expected. Additionally, the CCSD(T) values overall decrease in comparison to the MP2 CBS extrapolated results. This is expected as CCSD(T) is more accurate than MP2 and will present values closer to the CBS limit. An irregularity, however, is seen for the CCSD(T) EA value for the Cl . . . methanol neutral with C_s symmetry. The EA value is higher than the VDE energy, which should not be the case as the EA represents the ground state to ground state transition. This is due to the fact that there are two neutral states. The VDE is a transition from the anion potential energy surface to one of the neutral potential energy surfaces, while the EA is from the anion potential energy surface to the other neutral potential energy surface, resulting in a higher EA than the VDE. Furthermore, when comparing the calculated values and the experimental values, they do not compare favourably.

Table 3.2: Electronic energies for the chloride - methanol complex. The values in parenthesis represent uncertainty in the peak position, as determined by full width at half the maximum height

	D_0	VDE (eV)		EA (eV)		E_{stab}
	(kJ mol^{-1})	$^2P_{3/2}$	$^2P_{1/2}$	$^2P_{3/2}$	$^2P_{1/2}$	(eV)
MP2						
Cl^- ... methanol - C_s symmetry	68.3	4.38	4.49	-	-	-
Cl ... methanol - C_s symmetry	5.1	-	-	4.27	4.38	0.65
Cl ... methanol - C_1 symmetry	17.6	-	-	4.14	4.25	0.53
CCSD(T)						
Cl^- ... methanol - C_s symmetry	66.4	4.18	4.29	-	-	-
Cl ... methanol - C_s symmetry	4.9	-	-	4.25	4.36	0.64
Cl ... methanol - C_1 symmetry	19.9	-	-	4.10	4.20	0.48
Experimental	-	4.58(7)	-	-	-	0.96(11)

This was to be expected as the experimental photoelectron spectrum had high levels of inaccuracy, as explained in the Experimental Results section. At this stage, the computational values should be taken as the more accurate values, and further work will need to be done experimentally to complement these computational results.

3.2.3 Bromide-Methanol Complexes

The Br^- ... methanol anion structure is similar to that of the Cl^- ... methanol complex, retaining its C_s symmetry, however the distance between the halide and hydrogen has increased to 2.202 Å and the angle the halide makes with the appended hydrogen and oxygen has decreased to 165.8°. This complex is shown in Figure 3.19. Once again, the methanol structure alters due to the addition of bromide, with the O-H bond elongating from 0.959 Å to 0.985 Å, a smaller elongation than that for the Cl^- ... methanol complex.

The neutral complexes for Br . . . methanol held the same structure as those for the Cl . . . methanol complex, with the bromine - hydrogen distance increasing for the C_s symmetry structure and the presented angle decreasing, while for the C_1 symmetry structure the bromine - oxygen distance and the presented angle increased. Figures 3.20 and 3.21 show these two complexes with values of interest included.

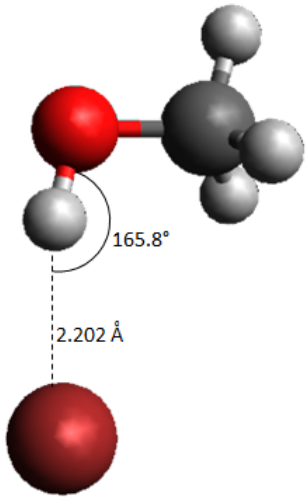

Figure 3.19: Br^- . . . methanol complex - C_s symmetry, optimised at the MP2/AVQZ level of theory

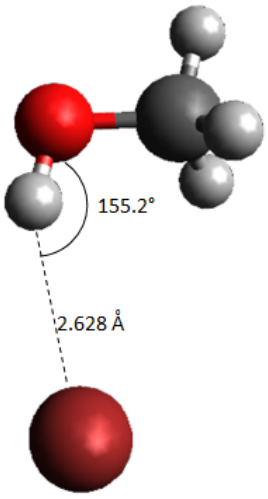

Figure 3.20: Br . . . methanol complex - C_s symmetry, optimised at the MP2/AVQZ level of theory

Table 3.3 lists the key energies, for both computational and experimental results. Once again, the CCSD(T) results decrease in energy compared to the MP2 results, as they are more accurate and approach the CBS limit. Unlike with chloride, the bromide energies show all EA values are lower than VDE values, as is expected. A comparison of the experimental and computational results shows much better correlation than for the chloride complexes. There is reasonable agreement between the VDE values and experimentally determined binding energies, with the CCSD(T) extrapolated VDE $^2P_{3/2}$ matching almost exactly. The CCSD(T) calculations for the E_{stab} values underestimate by approximately 100-200 meV. The calculations however provide a good estimate of the scale of the experimental E_{stab} values, providing a starting point for experimental methods.

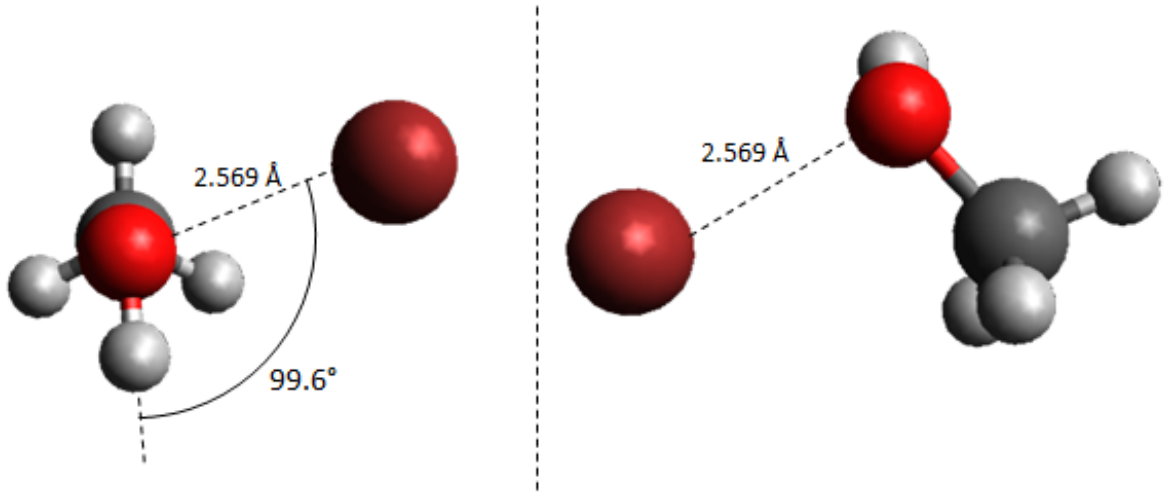

Figure 3.21: Br . . . methanol complex - C_1 symmetry (L: Front view, R: Top view), optimised at the MP2/AVQZ level of theory

Table 3.3: Electronic energies for the bromide - methanol complex. The values in parenthesis represent uncertainty in the peak position, as determined by full width at half the maximum height

	D_0	VDE (eV)		EA (eV)		E_{stab}
	(kJ mol^{-1})	$^2P_{3/2}$	$^2P_{1/2}$	$^2P_{3/2}$	$^2P_{1/2}$	(eV)
MP2						
Br^- . . . methanol - C_s symmetry	64.0	4.02	4.47	-	-	-
Br . . . methanol - C_s symmetry	7.6	-	-	3.95	4.41	0.58
Br . . . methanol - C_1 symmetry	20.4	-	-	3.82	4.27	0.45
CCSD(T)						
Br^- . . . methanol - C_s symmetry	63.7	4.00	4.46	-	-	-
Br . . . methanol - C_s symmetry	16.4	-	-	3.85	4.31	0.49
Br . . . methanol - C_1 symmetry	23.5	-	-	3.78	4.24	0.42
Experimental	-	4.00(11)	4.38(4)	-	-	0.64(26) ($^2P_{3/2}$) 0.57(28) ($^2P_{1/2}$)

Comparisons for the bromide energies to the chloride energies show that the values are sim-

ilar, with the same order of magnitude, with the anion D_0, E_{stab} and VDE's decreasing for bromide, while the neutral D_0 increased for both bromine structures. However, one irregularity is seen for the D_0 energy value given for the Br ... methanol neutral structure with C_s symmetry. This value shows at approximately 9 kJ mol^{-1} higher for CCSD(T) than its MP2 counterpart predicted. One possible reason for the unusual CCSD(T) D_0 value is due to bromine having an unusual polarisability versus its atomic size. As bromine is larger than chlorine, it has increased dispersion interaction, however its larger atomic size does not allow it to get closer to methanol. While iodine has a larger polarisability, its atomic radius places it further from methanol, and its interactions are therefore smaller. The balance between these two effects, polarisability and atomic radius, is a possible reason bromine has a greater binding strength than chlorine, and also iodine, as is shown in the next section. This anomalous value requires further investigation.

3.2.4 Iodide-Methanol Complexes

Iodide complexes follow the same general trend as observed for the bromide complexes, with the halide - hydrogen bond increasing to 2.471 Å and the halide - hydrogen - oxygen angle decreasing to 163.3° for the I$^-$ ... methanol anion structure shown in Figure 3.22. This trend of decreasing bond angle can be attributed to the increasing attraction between the methyl hydrogens and the halide. Another trend is observed with the O-H bond once more lengthening from 0.959 Å to 0.980 Å due to the addition of iodide. This bond elongation is a feature for all three halides, with the O-H bond length following the trend Cl $>$ Br $>$ I. This is expected as the D_0 value decreases as halide size increases, as presented in previous subsections and to be presented in Table 3.4. A decrease in D_0 values indicates that the complex becomes less stable as the halide size increases. Therefore, as the Cl$^-$ ... methanol complex is more stable the attraction between chloride and the oxygen appended hydrogen is stronger, resulting in a larger elongation. This O-H bond trend is also reflected in the vibrational frequencies. The O-H stretch for the three halides follows the trend Cl $<$ Br $<$ I, which indicates that Cl has a larger red shift than Br, which in turn has a larger red shift than I. A larger red shift implies a weaker bond, and thus the O-H bond and vibrational frequencies trends correlate.

The neutral iodine - methanol complexes have similar structures to the chlorine - methanol and bromine - methanol complexes, however the halogen - hydrogen distance has increased to 2.783 Å for the C_s symmetry structure and the halogen - oxygen distance has increased to 2.766 Å for the C_1 symmetry structure, while the presented angles have once again decreased for C_s and increased for C_1, as shown in Figures 3.23 and 3.24. The increase in angle size for the C_1 symmetry structure is due to the halide interaction with the oxygen appended hydrogen.

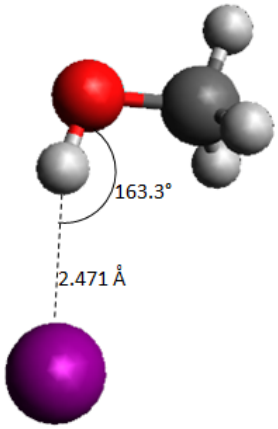

Figure 3.22: I^- ... methanol complex - C_s symmetry, optimised at the MP2/AVQZ level of theory

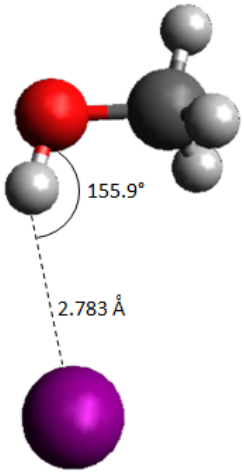

Figure 3.23: I ... methanol complex - C_s symmetry, optimised at the MP2/AVQZ level of theory

The energies calculated are presented in Table 3.4. Unfortunately, time did not permit for the I ... methanol - C_1 symmetry CCSD(T) single point energy calculations to run to completion, and so those results are omitted. Once more, the CCSD(T) extrapolated energies are lower than the MP2 energies as they approach the CBS limit. For iodide - methanol complexes, no irregularities were found in the results. The experimentally determined binding energies have reasonable agreement with the calculated VDE, and the calculated E_{stab} provides a good estimate of the experimental E_{stab}, once again underestimating by about 100 meV.

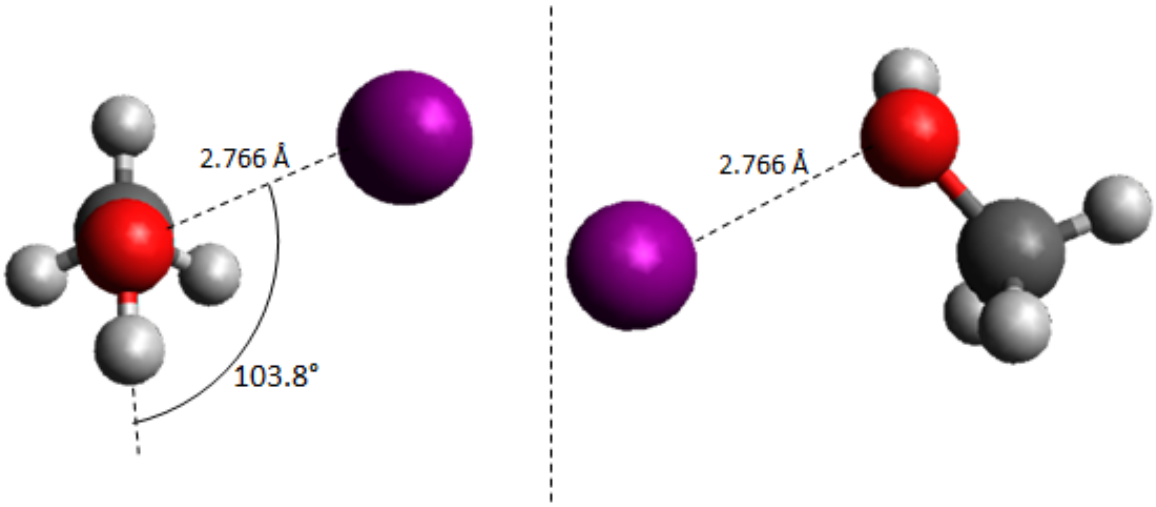

Figure 3.24: I . . . methanol complex - C_1 symmetry - (L: Front view, R: Top view), optimised at the MP2/AVQZ level of theory

Table 3.4: Electronic energies for the iodide - methanol complex. The values in parenthesis represent uncertainty in the peak position, as determined by full width at half the maximum height

	D_0	VDE (eV)		EA (eV)		E_{stab}
	(kJ mol^{-1})	$^2P_{3/2}$	$^2P_{1/2}$	$^2P_{3/2}$	$^2P_{1/2}$	(eV)
MP2						
I^- . . . MeOH - C_s symmetry	58.8	3.56	4.51	-	-	-
I . . . MeOH - C_s symmetry	11.9	-	-	3.55	4.49	0.49
I . . . MeOH - C_1 symmetry	25.3	-	-	3.41	4.35	0.35
CCSD(T)						
I^- . . . MeOH - C_s symmetry	53.8	3.55	4.49	-	-	-
I . . . MeOH - C_s symmetry	10.7	-	-	3.51	4.45	0.45
I . . . MeOH - C_1 symmetry *	-	-	-	-	-	-
Experimental	-	3.62(12)	4.53(3)	-	-	0.55(29) ($^2P_{3/2}$) 0.51(12) ($^2P_{1/2}$)

* Results not obtained due to time constraints

The iodide - methanol complexes continue the trend that as halide size increases, the anion D_0 value decreases, while the neutral D_0 value increases, bar the irregular bromine neutral for the C_s symmetry at the CCSD(T) extrapolation. This then explains the decrease in VDE and E_{stab}, as a decrease in anion D_0 and increase in neutral D_0 brings the two potential energy surfaces closer together.

3.2.5 Summary of Computational Results

All halide - methanol complexes optimised to similar geometries for the C_s anion complex and C_s and C_1 neutral complexes. As the halide size increases, the D_0 value decreases for the anion geometry. This suggests that the anion complexes become less stable and can be attributed to the increasing distance between the halide and methanol and decreasing charge density. Alternatively, the neutral D_0 values increased for increasing halide size. This is due to increased number of electrons as the halide size increases, increasing the dispersion forces between the halogen and methanol and increasing the complexes' stability. This is excluding the anomalous bromine complex, which had an unusual result, one possibility being due to the balance between its polarisability and atomic radius. This requires further investigation.

For all halogen - methanol complexes, the C_1 neutral structure was found to be more stable than the C_s neutral structure, as implied by the higher D_0 for the C_1 structure. Additionally, the relativity large D_0 values, for both anion and neutral structures, compared to previous Wild group experiments that will be discussed in the next section, could be a factor in atmospheric reactions.

The MP2 and CCSD(T) extrapolations provided similar results, with CCSD(T) energies lowering closer to the CBS limit for all halides. With the exclusion of the chloride - methanol complexes due to error in experiment, the VDE's calculated provided reasonable agreement with experimentally determined binding energies. The E_{stab}'s calculated across bromide and iodide underestimated the experimental E_{stab}'s by 100-200 meV, however provide reasonable estimates for experimental trends. For more accurate computational results, extrapolations at higher levels of theory are needed.

3.3 Comparison with Literature

In the previous section, D_0 was calculated for all halide - methanol anions and neutrals, and optimised geometries presented. Previous work has been reported by Hiraoka and Yamabe[7] and Hiraoka and Mizuse[38] that can be compared to the results obtained. Presented below in Table 3.5 are the calculated D_0 values alongside the literature experimental change in enthalpies and theoretically determined binding energies. Table 3.6 shows the comparison of geometries optimised in this project versus those optimised in literature.

Table 3.5: Calculated D_0 values compared to literature experimentally determined -$\triangle$H$^\circ$ and theoretically determined D_0

Cluster	Calculated D_0 (kJ mol^{-1})	Literature D_0 * (kJ mol^{-1})	Literature -$\triangle$H$^\circ$ * (kJ mol^{-1})
Cl^- ... methanol	66.4	67.8	72.8
Br^- ... methanol	63.7	66.9	58.2
I^- ... methanol	53.8	45.2	46.9

* Values obtained from Refs. 7,38.

Comparing the calculated D_0 values to literature, it can be noted that Cl^- ... methanol and Br^- ... methanol are in relative agreement, with the calculated values being lower than literature. This is expected, as this project calculated energies at CCSD(T) AVTZ/AVQZ extrapolation, while Hiraoko et al. performed ab initio MO calculations using the 3-21G basis set. As this project used a higher level of theory for calculations, the results are expected to be more accurate and the D_0 values showing lower than the literature values confirms this. Interestingly, the I^- ... methanol D_0 value is significantly larger than the literature value. This could be due to the two differing levels of theory, however the other two complexes produced similar

Table 3.6: Calculated optimised geometries compared to literature optimised geometries for all halide ... methanol complexes

	X^- ... H (Å)		∠X^- - H - O (°)	
Cluster	Calculated	Literature*	Calculated	Literature*
Cl^- ... methanol	2.075	2.26	167.1	163.2
Br^- ... methanol	2.202	2.39	165.8	162.4
I^- ... methanol	2.471	2.82	163.3	160.4

* Values obtained from Ref. 7.

results. The I^- ... methanol calculations were all checked and no errors in data analysis were observed, so more investigation is needed and calculations re-run to rule out error in calculations as the cause. A comparison of calculated values to experimentally determined binding energies shows a difference of 5-7 kJ mol^{-1}. This difference is expected as experiment and calculations operate at different temperatures. However, the calculations provide a good estimate for the trend in experimental binding energies.

Optimised parameters are compared to literature results in Table 3.6. The calculated X^- ... H bond length was consistently smaller than that found by Hiraoka and Yamabe,[7] while the ∠X^- - H - O calculated was consistently larger than that from literature. This difference is to be expected due to differing levels of theory, as Hiraoka and Yamabe performed ab initio MO calculations using the 3-21G basis set while the structures presented in this thesis are optimised at the MP2/AVQZ level of theory. However, the geometries optimised in this project had a similar structure to the geometries optimised by Hiraoka and Yamabe, and the trend of increasing X^- ... H bond and decreasing ∠X^- - H - O as the halide size increases is confirmed by literature.

The D_0 values calculated proved to be relatively large. As previously stated, work in the Wild group has been completed using the methods outlined above, including looking at halide -

nitrogen,[9] halide - acetone,[10] halide - formaldehyde[10] and halide - ethylene[11] clusters. A comparison of the D_0 and E_{stab} energies in these works compared to those calculated in this work for the I^- ... methanol complex is presented in Table 3.7 .

Table 3.7: Comparison of D_0 and E_{stab} calculated values for iodide complexes

Iodide complex	D_0 (kJ mol^{-1})	E_{stab} (eV)
Nitrogen	7.0	0.02
Ethylene (T-anion)	17.4	0.08
Ethylene (Bent-anion)	17.9	
Formaldehyde	43.3	0.26 (O-appended)
		0.41 (C-appended)
Methanol	53.8	0.45
Acetone	54.3	0.26

It is evident while comparing to past works that the D_0 value for the I^-... methanol complex is relatively high, as only one other complex surpasses methanol. Another clear trend is that as D_0 increases, E_{stab} increases, bar the acetone value (however it is noted in Reference 10 that E_{stab} values calculated were underestimated by approximately 200-300 mEV[10]). This is to be expected as increasing D_0 brings increasing stability to the complex, and a higher E_{stab} means increasing stability for the electron on the complex compared to the bare halide. The methanol complex is closer in energy to formaldehyde and acetone, due to the presence of oxygen. Oxygen creates a strong dipole, therefore formaldehyde, methanol and acetone complexes are more strongly bound and have an increased D_0 value.

Chapter 4

Conclusion and Future Work

The aims of this project were to study the ways in which halides interacted with the simplest alcohol, methanol. A TOF-MS/PES apparatus was used to obtain mass spectra and, for the first time, photoelectron spectra for Cl^- ... methanol, Br^- ... methanol and I^- ... methanol clusters. High level calculations provided energies, geometries and vibrational frequencies to complement the experimental results. This work has added to our understanding of the halogen - methanol potential energy surface, which can lead to an enhanced understanding of reaction pathways.

From the photoelectron spectra produced, electron binding energies for all halide - methanol complexes were found from the peaks. The electron binding energy of the $^2P_{3/2}$ state for the Cl^- ... methanol complex was found to be 4.58(7) eV, while the electron binding energies for the $^2P_{3/2}$ state and $^2P_{1/2}$ state for the Br^- ... methanol and I^- ... methanol complexes were 4.00(11) eV, 4.38(4) eV and 3.62(12) eV, 4.53(3) eV respectively. E_{stab} values were also calculated for all complexes by determining the difference in electron binding energies between the bare halide ion and the anion complex, with the values ranging from 0.51(12) eV (I^- ... methanol) to 0.96(11) eV (Cl^- ... methanol). This indicates that the electron is more strongly bound for the halide complexes compared with the bare halides.

Experimental data were supported through ab initio calculations, which were performed to determine geometries, energies and vibrational frequencies of all halide - methanol and halogen - methanol complexes. Geometries were optimised to the MP2/AVQZ level of theory, with single point energies calculated using these geometries up to the CCSD(T)/AVQZ level of theory. One halide - methanol geometry was elucidated, with a C_s symmetry where the halide sits in line with the O-H bond. The binding energy of this complex was found to be relatively high compared to other complexes studied in the Wild group, having a binding energy similar in magnitude to other oxygen containing species. Two halogen - methanol complexes were found, one with a C_s symmetry once again with the halide in line with the O-H bond, and one with a C_1 symmetry, where the halide sits either to the left or right of the oxygen. The C_1 symmetry structure had a significantly higher D_0 value, making it more stable.

The computational results provided values for E_{stab} and VDE that provided good estimates and similar trends to experimentally determined E_{stab} and binding energies. However, a problem arose when calculated VDE's mapped onto the lower neutral surface, providing EA's that were higher than VDE's, which should not occur. This provides an avenue for future work, for calculating the VDE's at different levels of theory and basis sets, hopefully improving on the accuracy of these results. Another possibility would be to optimise the structures at a higher level of theory, and then perform the CBS extrapolation again, improving accuracy of results, and hopefully improving experiment to computation comparisons.

To better improve the computational results, future work would involve completing the geometry optimisations and performing single point energies at a higher level of theory. It would also be advised to study the halide - methanol structure that was found in the 1-D scan, where the halide sat in the methyl pocket. While this structure was omitted due to time limiting the opportunities to investigate this structure at a level of theory higher than CCSD(T)/AVDZ, future studies should be done to see if this structure does optimise at higher levels.

Future directions for the experimental side of this project would begin with the chloride - methanol photoelectron spectrum being investigated again. Unfortunately the apparatus was not functioning optimally when the spectrum was taken, and therefore retaking spectrum now that the apparatus is operating smoothly is advised. To further the PES experimental results, experiments using a slow electron velocity-map imaging (SEVI) apparatus would increase accuracy. SEVI is similar to PES, however it has a higher resolution. During PES experiments, a photon provides large amounts of energy to photo-detach electrons, resulting in a large range of vibrational states for studying, with the disadvantage of low resolution. SEVI works by a photon providing just enough energy for a small band width of electrons to photo-detach, resulting in less vibrational states for studying, but a higher resolution.[39] The Wild group is in the process of getting such an apparatus up and running.

References

[1] Hobza,P; Muller-Dethlefs, K. *Noncovalent Interactions: Theory and Experiment*; The Royal Society of Chemistry: U.K, 2009.

[2] Anderson, J. G.; Toohey, D. W.; Brune, W.H. Free Radicals Within the Antarctic Vortex: The Role of CFCs in Antarctic Ozone Loss. *Science*. **1991**, *251*, 39-46.

[3] Von Glasow, R.; Sander, R. Modeling Halogen Chemistry in the Marine Boundary Layer. *J. Geo. Phys. Research.* **2002**, *107*, **ACH 9** - 1-16.

[4] Simpson, W.R.; Brown, S.S; Saiz-Lopez. A.; Thornton, J.A.; Von Glasow. R. Tropospheric Halogen Chemistry: Sources, Cycling, and Impacts. *Chem. Rev.* **2015**, *115*, 4035-4062.

[5] Galbally, I.E.; Kirstine, W. The Production of Methanol by Flowering Plants and the Global Cycle of Methanol. *J. Atmos. Chem.* **2002**, *43*, 195-229.

[6] Markovich, G.; Pollack, S.; Giniger, R.; Cheshnovsky, O. Photoelectron Spectroscopy of Cl-, Br-, and I- Solvated in Water Clusters. *J. Chem. Phys.* **1994**, *101*, 9344 - 9353.

[7] Hiraoka, K; Yamabe, S. Solvation of Halide Ions with CH_3OH the Gas Phase. *Int. J. Mass Spectrm. Ion Process.* **1991**, *109*, 133-150.

[8] Draves, J.A.; Luthey-Schulten, Z.; Lui, W.; Lisy J.M. Gas-phase Methanol Solvation of Cs^+: Vibrational Spectroscopy and Monte Carlo Simulation. *J. Chem. Phys.* **1990**, *93*, 4589-4602.

[9] Lapere, K.M.L.; Kettner, M.; Watson, P.D.; McKinley, A.J.; Wild, D.A. The Halide-Nitrogen Gas-Phase Clusters: Anion Photoelectron Spectroscopy and High Level Ab Initio Calculations. *J. Phys. Chem. A.* **2015**, *119*, 9722-9728.

[10] Corkish, T. Interactions Between Halogens and the Simplest Carbonyls, Formaldehyde and Acetone. BSc Honours Thesis, University of Western Australia, Perth, W.A., 2016.

[11] t' Hart, D. Halogens and the Carbon-Carbon Double Bond: Spectroscopy and Theory. BSc Honours Thesis, University of Western Australia, Perth, W.A., 2016.

[12] Young, R.M.; Yandell, M.A.; Neumark, D.M. Dynamics of Electron Solvation in $I^-(CH_3OH)_n$ Clusters $(4 \leq n \leq 11)$. *J. Chem. Phys*. **2011**, *134*, 124311-1 - 124311-10.

[13] Mak, C.C.; Peslherbe, G.H. Relaxation Pathways of Photoexcited Iodide-Methanol Clusters: A Computational Investigation. *J. Phys. Chem. A.* **2014**, *118*, 4494-4501.

[14] Robertson, W.H.; Karapetian, K; Ayotte, P.; Jordan, K.D.; Johnson, M.A. Infrared Predissociation Spectroscopy of $I^-(CH_3OH)_n$, n=1,2: Cooperatively in Asymmetric Solvation. *J. Chem. Phys.* **2002**, *116*, 4853-4857.

[15] Corbett, C.A.; Martinez, T.J.; Lisy, J.M. Solvation of the Fluoride Anion by Methanol. *J. Phys. Chem. A.* **2002**, *106*, 10015-10021.

[16] Cabarcos, O.M.; Weinheimer, T.J.; Martinez, T.J.; Lisy, J.M. The Solvation of Chloride by Methanol - Surface Versus Interior Cluster Ion States. *J. Chem. Phys.* **1999**, *110*, 9516-9526.

[17] Ayala, R.; Martinez, J.M.; Pappalardo, R.R.; Marcos, E.S. Theoretical Study of the Microsolvation of the Bromide Anion in Water, Methanol and Acetonitrile: Ion - Solvent vs Solvent - Solvent Interactions. *J. Phys. Chem. A.* **2000**, *104*, 2799-2807.

[18] Lapere, K.M.L. Anion Photoelectron Spectroscopy of Halide Complexes and Clusters. Ph.D. Thesis, University of Western Australia, Perth, W.A., 2015.

[19] Kettner, M. Aspects of Gas-Phase Anion Spectroscopy. Ph.D. Thesis, University of Western Australia, Perth, W.A., 2015.

[20] Lewars, E.G. *Computational Chemistry: Introduction to the Theory and Applications of Molecular and Quantum Mechanics*, 2nd Ed.; Springer Netherlands: Dordrecht, 2011.

[21] Hasanein, A. A.; Evans, M. W. *Computational Methods in Quantum Chemistry, Vol.2: Quantum Chemistry*; World Scientific Publishing: Singapore, 1996.

[22] Jung, Y.; Lochan, R.C.; Dutoi, A.D.; Head-Gordon, M. Scaled Opposite-spin Second Order Mϕller-Plesset Correlation Energy: An Economical Electronic Structure Method. *J. Chem. Phys.* **2004**, *121*, 9793-9802.

[23] Dunning, Jr., T.H. Gaussian Basis Sets for Use in Correlated Molecular Calculations. I. The Atoms Boron Through Neon and Hydrogen. *J. Chem. Phys.* **1989**, *90*, 1007-1023.

[24] Kendall, R.A.; Dunning, Jr., T.H.; Harrison, R.J. Electron Affinities of the First- row Atoms Revisited. Systematic Basis Sets and Wave Functions. *J. Chem. Phys.* **1992**, *96*, 6796-6806.

[25] Woon, D.E.; Dunning, Jr., T.H. Gaussian Basis Sets for Use in Correlated Molecular Calculations. III. The Atoms Aluminium Through Argon. *J. Chem. Phys.* **1993**, *98*, 1358-1371.

[26] Dunning, Jr., T. H.; Peterson, K.A.; Wilson, A.K. Gaussian Basis Sets for Use in Correlated Molecular Calculations. X. The Atoms Aluminium Through Argon Revisited. *J. Chem. Phys.* **2001**, *114*, 9244-9253.

[27] Peterson, K.A.; Figgen, D.; Goll, E.; Stoll, H.; Dolg, M. Systematically Convergent Basis Sets with Relativistic Pseudopotentials. II. Small-core Pseudopotentials and Correlation Consistent Basis Sets for the Post-d Group 1618 Elements. *J. Chem. Phys.* **2003**, *119*, 11113.

[28] Wiley, W.C.; McLaren, I.H. Time-of-Flight Mass Spectrometer with Improved Resolution. *Rev. Sci. Instrum.* **1955**, *26*, 1150-1157.

[29] Lapere, K.M.L.; LaMacchia, R.J.; Quak, L.H.; McKinley, A.J.; Wild, D.A. Anion Photoelectron Spectroscopy and ab initio Calculations of the Gas Phase Chloride - Carbon Monoxide Complex: $Cl^-\ldots CO$. *Chem. Phys. Lett.* **2011**, *504*, 13-19.

[30] Zipf, E.C. *Electron Molecule Interactions and their Applications. Ch. 4: Dissociation of Molecules by Electron Impact* Vol. 1. Academic Press Inc.: Orlando, Florida, 1984.

[31] Bartmess, J.E. "Negative Ion Energetics Data" in **NIST Chemistry WebBook, NIST Standard Reference Database Number 69**, Linstrom, P. J.; Mallard, W. G. Eds., National Institute of Standards and Technology, Gaithersburg MD, 20899.

[32] Gaussian 09, Revision D.01, Frisch, M. J.; Trucks, G. W.; Schlegel, H. B.; Scuseria, G. E.; Robb, M. A.; Cheeseman, J. R.; Scalmani, G.; Barone, V.; Petersson, G. A.; Nakatsuji, H.; Li, X.; Caricato, M.; Marenich, A.; Bloino, J.; Janesko, B. G.; Gomperts, R.; Mennucci, B.; Hratchian, H. P.; Ortiz, J. V.; Izmaylov, A. F.; Sonnenberg, J. L.; Williams-Young, D.; Ding, F.; Lipparini, F.; Egidi, F.; Goings, J.; Peng, B.; Petrone, A.; Henderson, T.; Ranasinghe, D.; Zakrzewski, V. G.; Gao, J.; Rega, N.; Zheng, G.; Liang, W.; Hada, M.; Ehara, M.; Toyota, K.; Fukuda, R.; Hasegawa, J.; Ishida, M.; Nakajima, T.; Honda, Y.; Kitao, O.; Nakai, H.; Vreven, T.; Throssell, K.; Montgomery, J. A.; Peralta, Jr., J. E.; Ogliaro, F.; Bearpark, M.; Heyd, J. J.; Brothers, E.; Kudin, K. N.; Staroverov, V. N.; Keith, T.; Kobayashi, R.; Normand, J.; Raghavachari, K.; Rendell, A.; Burant, J. C.; Iyengar, S. S.; Tomasi, J.; Cossi, M.; Millam, J. M.; Klene, M.; Adamo, C.; Cammi, R.; Ochterski, J. W.; Martin, R. L.; Morokuma, K.; Farkas, O.; Foresman, J. B. and Fox, D. J. Gaussian, Inc., Wallingford CT, 2013.

[33] Schuchardt, K. L.; Didier, B. T.; Elsethagen, T.; Sun, L.; Gurumoorthi, V.; Chase, J.; Li, J.; Windus, T. L. *J. Chem. Inf. Model.* **2007**, *47*, 10451052

[34] Stanton, J. F.; Gauss, J.; Harding, M. E.; Szalay, P. G. CFOUR, Coupled-Cluster Techniques for Computational Chemistry.

[35] Karton, A.; Martin, J. Comment on: Estimating the HartreeFock limit from finite basis set calculations [Jensen F (2005) Theor Chem Acc 113:267]. *Theor. Chem. Acc.* **2006**, *115*, 330-333.

[36] Helgaker, T.; Klopper, W.; Koch, H; Noga, J. Basis set convergence of correlated calculations on water. *J. Chem. Phys.* **1997**, *106*, 9639-9646.

[37] Karton, A.; Martin, J. Explicitly correlated Wn theory: W1-F12 and W2-F12. *J. Chem. Phys.* **2012**, *136*, 124114.

[38] Hiraoka, K; Mizuse, S. Gas-phase solvation of Cl^- with H_2O, CH_3OH, C_2H_5OH, $i{-}C_3H_7OH$, $n{-}C_3H_7OH$ and $t{-}C_4H_9OH$. *Chem. Phys.* **1987**, *118*, 457-466.

[39] Neumark, D.M. Slow Electron Velocity-Map Imaging of Negative Ions: Applications to Spectroscopy and Dynamics. *J. Phys. Chem. A.* **2008**, *112*, 13287-13301.

Appendix A

Data and Tables

Appendix A includes tables of computational data obtained, including geometries, vibrational frequencies and intensities, and calculated energies at MP2 and CCSD(T) levels of theory.

Table A.1: Cartesian coordinates of the geometry of methanol optimised at the MP2/aug-cc-pVQZ level of theory

	x	y	z
C	0.04657	0.66412	0.00000
O	0.04657	-0.75575	0.00000
H	-0.43683	1.07118	0.88789
H	-0.43683	1.07118	-0.88789
H	1.08581	0.97378	0.00000
H	-0.86416	-1.05482	0.00000

Table A.2: Energies of the methanol molecule at MP2 and CCSD(T) levels of theory using the MP2 geometries

MP2 E_h (Hartree)				zpe
TZ	QZ	5Z	CBS	(kJ mol^{-1})
-115.528989	-115.563112	-115.575354	-115.101987	136.5
CCSD(T) E_h (Hartree)				
DZ	TZ	QZ	CBS	
-115.455073	-115.562308	-115.593161	-115.610769	-

Table A.3: Vibrational frequencies and intensities for the methanol molecule at the MP2/aug-cc-pVQZ level of theory

Vibrational Frequency	Intensity
cm^{-1}	km mol^{-1}
296	104.5
1061	116.7
1093	3.3
1187	0.4
1373	21.1
1491	3.2
1524	3.2
1534	5.4
3058	53.2
3131	38.6
3190	18.1
3878	41.3

Table A.4: Cartesian coordinates of the geometries of halide - methanol complexes optimised at MP2/aug-cc-pVQZ (pV(Q+d)Z for Cl and pVQZ-PP for Br and I)

Cl^- ... methanol				Br^- ... methanol				I^- ... methanol			
	x	y	z		x	y	z		x	y	z
C	-1.88106	0.33353	0.00000	C	0.60337	-2.41842	0.00000	C	0.61711	-2.83852	0.00000
O	-0.82771	1.26888	0.00000	O	-0.73008	-1.97052	0.00000	O	-0.73899	-2.45382	0.00000
H	-1.85535	-0.31323	0.88274	H	1.15032	-2.07433	0.88125	H	1.14551	-2.46936	0.88148
H	-1.85535	-0.31323	-0.88274	H	1.15032	-2.07433	-0.88125	H	1.14551	-2.46936	-0.88148
H	-2.82258	0.88662	0.00000	H	0.58981	-3.50823	0.00000	H	0.64909	-3.92717	0.00000
H	0.00000	0.72377	0.00000	H	-0.66999	-0.98610	0.00000	H	-0.73084	-1.47405	0.00000
Cl	1.43772	-0.77272	0.00000	Br	0.00000	1.11193	0.00000	I	0.00000	0.88682	0.00000

Table A.5: Energies of the halide - methanol complexes at MP2 and CCSD(T) levels of theory using the MP2 geometries

Complex	MP2 E_h (Hartree)				zpe	Corrected zpe*
	TZ	QZ	5Z	CBS	(kJ mol^{-1})	(kJ mol^{-1})
Cl^- ... methanol	-575.337777	-575.393170	-575.413802	-575.433425	138.6	2.8
Br^- ... methanol	-531.372737	-531.485844	-531.584978	-531.687291	138.2	2.1
I^- ... methanol	-410.516883	-410.631856	-410.704424	-410.778904	138.2	1.6
	CCSD(T) E_h (Hartree)					
	DZ	TZ	QZ	CBS		
Cl^- ... methanol	-575.224796	-575.395737	-575.447881	-575.478288	-	-
Br^- ... methanol	-531.204653	-531.423526	-531.530358	-531.595637	-	-
I^- ... methanol	-410.358392	-410.566045	-410.675675	-410.742060	-	-

* Including only the van der Waals intermolecular modes

Table A.6: Vibrational frequencies and intensities for the chloride - methanol, bromide - methanol and iodide - methanol complexes at the MP2/aug-cc-pVQZ level of theory (pV(Q+d)Z for Cl and pVQZ - PP for Br and I)

Cl^- ... methanol		Br^- ... methanol		I^- ... methanol	
Vibrational Frequency	Intensity	Vibrational Frequency	Intensity	Vibrational Frequency	Intensity
cm^{-1}	km mol^{-1}	cm^{-1}	km mol^{-1}	cm^{-1}	km mol^{-1}
121	14.3	57	0.1	76	< 0.1
129	< 0.1	100	5.2	92	3.1
223	17.0	200	4.4	167	0.9
814	43.2	761	33.9	681	29.7
1091	78.9	1098	75.7	1090	70.6
1138	7.0	1130	8.9	1123	11.6
1189	0.6	1189	0.5	1189	0.4
1473	5.0	1468	16.7	1445	19.3
1485	17.4	1473	4.7	1474	1.5
1503	2.0	1501	2.8	1503	4.1
1535	10.6	1532	12.5	1531	15.2
3006	133.6	3023	113.0	3031	85.9
3070	60.5	3088	54.7	3099	44.7
3101	96.8	3121	90.1	3132	80.2
3286	1216.6	3363	1174.8	3476	963.1

Table A.7: Cartesian coordinates of the geometries of halogen - methanol complexes (C_s symmetry) optimised at MP2/aug-cc-pVQZ (pV(Q+d)Z for Cl and pVQZ-PP for Br and I)

Cl . . . methanol				Br . . . methanol				I . . . methanol			
	x	y	z		x	y	z		x	y	z
C	1.95193	-0.57938	0.00002	C	-0.63979	-2.51988	0.00000	C	0.64067	-2.93940	0.00000
O	1.58317	0.79054	-0.00013	O	0.75019	-2.23772	0.00000	O	-0.75074	-2.66505	0.00000
H	1.58810	-1.09963	-0.88636	H	-1.13614	-2.12474	-0.88683	H	1.13504	-2.54120	0.88671
H	1.59078	-1.09871	0.88804	H	-1.13614	-2.12474	0.88683	H	1.13504	-2.54120	-0.88671
H	3.03616	-0.61129	-0.00160	H	-0.74029	-3.59998	0.00000	H	0.74705	-4.01902	0.00000
H	0.62455	0.83407	0.00110	H	0.84979	-1.28258	0.00000	H	-0.85524	-1.70973	0.00000
Cl	-1.83627	-0.05132	-0.00002	Br	0.00000	1.20437	0.00000	I	0.00000	0.93902	0.00000

Table A.8: Energies of the halogen - methanol complexes (C_s symmetry) at MP2 and CCSD(T) levels of theory using the MP2 geometries

Complex	MP2 E_h (Hartree)				zpe	Corrected zpe *
	TZ	QZ	5Z	CBS	(kJ mol^{-1})	(kJ mol^{-1})
Cl . . . methanol	-575.179591	-575.231824	-575.251151	-575.269344	137.4	1.0
Br . . . methanol	-531.224727	-531.333923	-531.431617	-531.532343	137.4	1.0
I . . . methanol	-410.379495	-410.490368	-410.560941	-410.633232	137.4	1.3
	CCSD(T) E_h (Hartree)					
	DZ	TZ	QZ	CBS		
Cl . . . methanol	-575.075820	-575.242776	-575.291417	-575.319280	-	-
Br . . . methanol	-531.056486	-531.279440	-531.382226	-531.447593	-	-
I . . . methanol	-410.228070	-410.432122	-410.537562	-410.601176	-	-

* Including only the van der Waals intermolecular modes

Table A.9: Vibrational frequencies and intensities for the chlorine - methanol , bromine - methanol and iodine - methanol complexes (C_s symmetry) at the MP2/aug-cc-pVQZ level of theory (pV(Q+d)Z for Cl and pVQZ - PP for Br and I)

Cl . . . methanol		Br . . . methanol		I . . . methanol	
Vibrational Frequency	Intensity	Vibrational Frequency	Intensity	Vibrational Frequency	Intensity
cm^{-1}	km mol^{-1}	cm^{-1}	km mol^{-1}	cm^{-1}	km mol^{-1}
35	2.2	43	9.3	51	1.1
42	11.6	44	1.7	64	8.7
86	0.9	87	1.0	99	1.2
309	91.5	317	86.9	319	77.8
1065	102.9	1065	97.8	1066	92.3
1096	5.9	1095	8.9	1095	10.3
1188	0.5	1188	0.5	1184	3.8
1382	18.7	1383	20.3	1383	19.9
1489	2.2	1488	1.7	1487	1.2
1522	4.2	1521	4.7	1514	2.9
1532	8.0	1530.0	9.8	1530	11.8
3053	49.8	3052	47.9	3051	45.3
3126	39.1	3124	38.2	3119	49.0
3186	23.0	3185	25.2	3184	27.2
3861	111.1	3844	138.1	3830	165.4

Table A.10: Cartesian coordinates of the geometries of halogen - methanol complexes (C_1 symmetry) optimised at MP2/aug-cc-pVQZ (pV(Q+d)Z for Cl and pVQZ-PP for Br and I)

Cl . . . methanol				Br . . . methanol				I . . . methanol			
	x	y	z		x	y	z		x	y	z
C	-1.71764	-0.46329	0.02308	C	-2.25587	-0.48495	0.02304	C	-2.65029	-0.49796	0.02308
O	-0.89494	0.69519	-0.13004	O	-1.47630	0.70289	-0.12905	O	-1.88332	0.69789	-0.12651
H	-2.75537	-0.17941	0.18651	H	-3.30887	-0.24295	0.15172	H	-3.71373	-0.27452	0.07769
H	-1.37030	-1.09075	0.84094	H	-1.90647	-1.08358	0.86175	H	-2.34401	-1.05934	0.90381
H	-1.63895	-1.01592	-0.90538	H	-2.12750	-1.05099	-0.89188	H	-2.45610	-1.09581	-0.85977
H	-0.89972	1.18486	0.69748	H	-1.53242	1.21101	0.68525	H	-2.01030	1.24157	0.65599
Cl	1.41939	-0.09886	0.00484	Br	0.97774	-0.04420	0.00249	I	0.78288	-0.02655	0.00181

Table A.11: Energies of the halogen - methanol complexes (C_1 symmetry) at MP2 and CCSD(T) levels of theory using the MP2 geometries

Complex	MP2 E_h (Hartree)				zpe	Corrected zpe *
	TZ	QZ	5Z	CBS	(kJ mol^{-1})	(kJ mol^{-1})
Cl . . . methanol	-575.184345	-575.236975	-575.256497	-575.274899	139.6	2.6
Br . . . methanol	-531.229683	-531.339386	-531.437148	-531.537947	139.3	2.3
I . . . methanol	-410.383930	-410.495441	-410.566303	-410.638887	138.9	2.1
	CCSD(T) E_h (Hartree)					
	DZ	TZ	QZ	CBS		
Cl . . . methanol	-575.081655	-575.248415	-575.297652	-575.325809	-	-
Br . . . methanol	-531.070110	-531.284769	-531.388203	-531.451021	-	-
I . . . methanol	-410.232482	-410.436453	**	**	-	-

* Including only the van der Waals intermolecular modes

** Results not obtained due to time constraints

Table A.12: Vibrational frequencies and intensities for the chlorine - methanol , bromine - methanol and iodine - methanol complexes (C_1 symmetry) at the MP2/aug-cc-pVQZ level of theory (pV(Q+d)Z for Cl and pVQZ - PP for Br and I)

Cl . . . methanol		Br . . . methanol		I . . . methanol	
Vibrational Frequency	Intensity	Vibrational Frequency	Intensity	Vibrational Frequency	Intensity
cm^{-1}	km mol^{-1}	cm^{-1}	km mol^{-1}	cm^{-1}	km mol^{-1}
114	0.9	104	0.3	93	0.5
130	0.5	124	1.8	114	3.8
184	36.9	168	28.1	150	21.6
427	115.1	413	116.7	385	120.2
1043	125.4	1044	121.7	1045	118.7
1078	3.8	1078	2.7	1080	1.7
1185	0.2	1185	0.1	1185	0.1
1359	14.5	1360	14.1	1362	13.6
1482	9.1	1483	6.5	1485	4.2
1520	6.4	1520	5.9	1520	5.8
1526	6.3	1526	7.4	1527	8.6
3075	42.4	3074	41.4	3072	40.2
3161	15.5	3159	17.8	3157	21.2
3209	8.5	3206	8.4	3203	8.6
3841	69.0	3841	66.2	3843	62.1

Appendix B

Schematic of TOF-MS/PES Timing

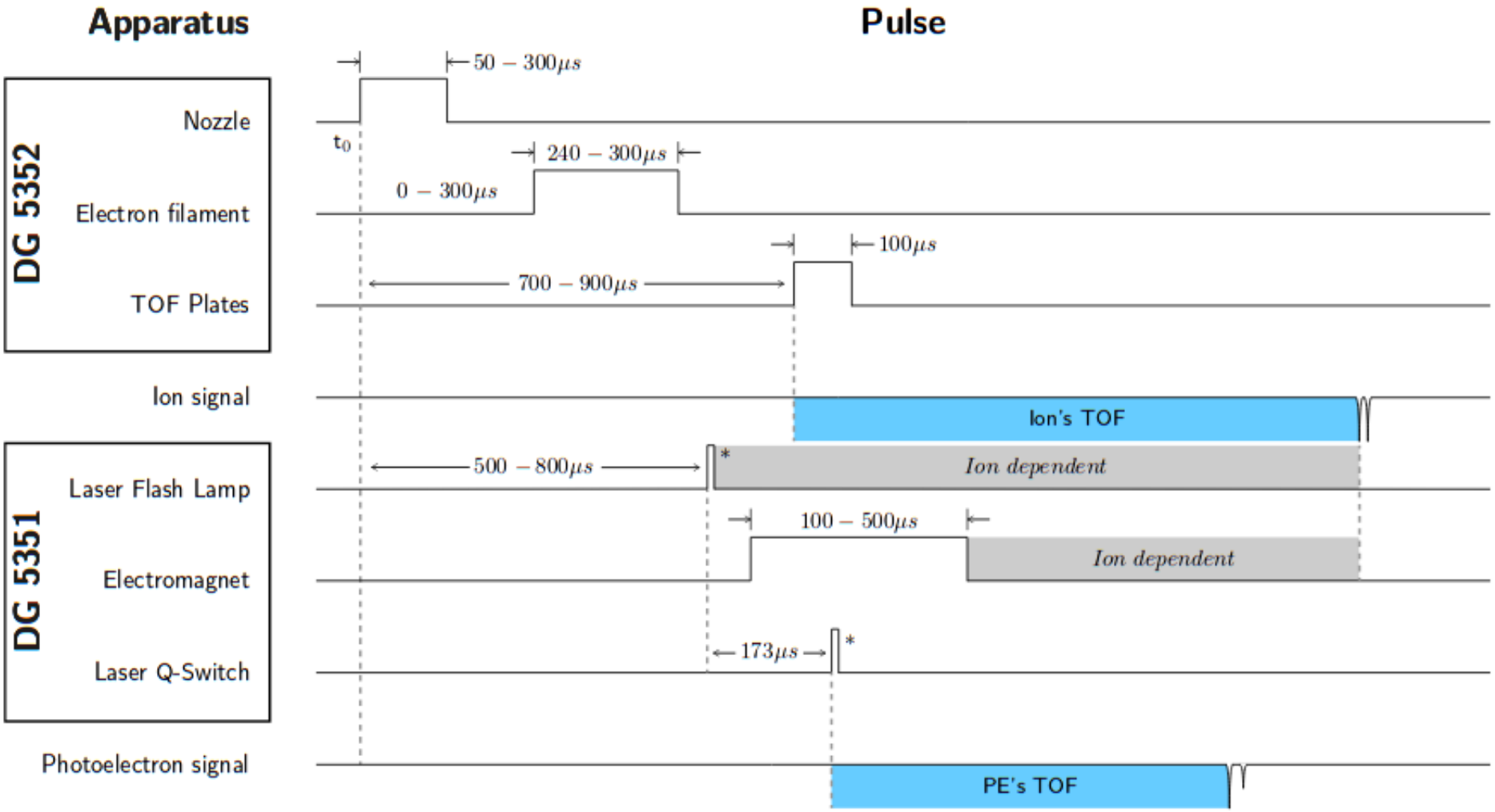

Figure B.1: Schematic displaying the relative timing of the various TOF-MS/PES components[18]